PERGAMON

International Journal of Solids and Structures 38 (2001) 2683–2711

INTERNATIONAL JOURNAL OF SOLIDS and STRUCTURES

www.elsevier.com/locate/ijsolstr

Microplane model for concrete with relaxed kinematic constraint

Joško Ožbolt [a,*], Yijun Li [a], Ivica Kožar [b]

[a] *Institute of Construction Materials, University of Stuttgart, Pfaffenwaldring 4, 70550 Stuttgart, Germany*
[b] *Faculty of Civil Engineering, University of Rijeka, V.C. Emina 5, 51000 Rijeka, Croatia*

Received 10 December 1996; in revised form 7 April 2000

Abstract

In the paper, the microplane material model for concrete based on the relaxed kinematic constraint is presented. The model is aimed to be used for three-dimensional damage and fracture analysis of concrete and reinforced concrete structures in the framework of smeared crack approach. In the microplane model, the material is characterized by a relation between the stress and strain components on planes of various orientations. These planes may be imagined to represent the damage planes or weak planes in the microstructure, such as contact layers between aggregate pieces in concrete. The tensorial invariance restrictions need not be directly enforced. They are automatically satisfied by superimposing in a suitable manner the responses from all the microplanes. To realistically model concrete under compressive load, for each microplane, the total strain tensor has to be decomposed into the normal (volumetric and deviatoric) and shear strain component. It is shown that for dominant tensile load the decomposition of the normal microplane strain into volumetric and deviatoric part, together with the fact that the tensile strength of concrete is an order of magnitude smaller than it's compressive strength, leads to unrealistic model response. To keep the conceptual simplicity, the model is improved in the framework of the kinematic microplane theory, however, the kinematic constraint at the microplane level is relaxed. The proposed approach finds its physical background in the discontinuity of the strain field. It is demonstrated that the improved model correctly predicts the concrete response for dominant tensile load. The implementation of the initial anisotropy and the modeling of concrete for cyclic loading is also discussed. Comparison with a number of test data for different stress–strain histories shows a good agreement. The model has been recently implemented into a two- and three-dimensional finite element code and coupled with the localization limiter of local (crack band) and nonlocal integral type.

Keywords: Macroscopic modeling; Concrete; Fracture; Microplane model; Discontinuity; Kinematic constraint; Initial anisotropy; Cyclic loading; Structural analysis

1. Introduction

In recent years, a significant effort in modeling of concrete-like materials for general stress–strain histories has been expended. Presently the available models for concrete can roughly be classified into two

* Corresponding author. Fax: +49-711-685-3349.
E-mail address: ozbolt@iwb.uni-stuttgart.de (J. Ožbolt).

0020-7683/01/$ - see front matter
PII: S0020-7683(00)00177-3

categories: (1) macroscopic models, in which the material behavior is considered to be an average response of a rather complex microstructural stress transfer mechanism and (2) the microscopic models, where the micromechanics of deformations is described by stress–strain relations on the microlevel. No doubt, from the physical point of view, more promising are microscopic models. However, they are computationally extremely demanding. Therefore, in practical applications we have to use macroscopic models.

At the macroscale, the model has to correctly describe microstructural phenomena such as cohesion, friction and aggregate interlock. These phenomena make the consumption of energy, which is released as a consequence of cracking, possible. They are microstructural (volume) and not point material properties. Consequently, the macroscopic models have to be related to the characteristic volume in which these phenomena take place i.e. they have to be nonlocal (Pijaudier-Cabot and Bažant, 1987; Bažant, 1991; de Borst, 1991; Ožbolt and Bažant, 1996). From the microscopic point of view (micro models), the nonlocality has no meaning. However, the same as the macroscopic model, itself, the nonlocality is an important tool (concept, model, etc.) which makes representation of the microscopic phenomena on the macroscale realistic. The problems of nonlocality and regularization procedures are beyond the scope of the present paper and are not discussed here in detail.

The evolution of damage (cracking) is closely related to the structure geometry and its size. Due to the fact that the material testing is performed on specimens of a finite size (structures), from experimental results it is difficult to filter out the macroscopic material properties. Typical example is the uniaxial compressive test. As soon as the peak load is reached (approximately uniaxial compressive strength), a number of vertical or inclined cracks arise. The specimen (structure) fails after smaller cracks result into one (or more) diagonal-shear-splitting crack(s), whose propagation is controlled by the specimen size and boundary conditions. In the critical (the weakest) cross section (crack plane), the material ruptures i.e. discontinuous change of the strain field takes place (continuum $\rightarrow$ discontinuum). Perpendicular to the discontinuity plane as well as in the three-dimensional space around it, the stresses and strains relax (unload) approximately to zero (Fig. 1).

Traditionally, the macroscopic models are formulated by total or incremental formulation between the σ_{ij} and ε_{ij} components of the stress and strain tensor, using the theory of tensorial invariants (Chen and Chen, 1975; Willam and Warnke, 1974; Gerstle et al., 1980; Gerstle, 1981; Ortiz, 1985). In the framework of the theory, there are various possible approaches for modeling of concrete, such as plasticity, plastic-fracturing theory, continuum damage mechanics, endocronic theory and their various combinations. Due to the complexity of the concrete, presently exists no model based on the stress and strain tensor and their invariants which is capable to realistically predict the behavior of concrete, not only for the three-dimensional monotonic loading, but also for the general three-dimensional cyclic loading. For instance, the invariant type of the models have difficulties with correct modeling of concrete expansion for triaxial compressive load, which in some applications governs the failure mechanism and is a consequence of cracking (discontinuity). Such models are based on the continuum mechanics and are generally not capable to simulate complex stress–strain states, which involve cracking, using only a few available invariants. Moreover, based on the plasticity type of the flow rules, which is most commonly in these models used, it is

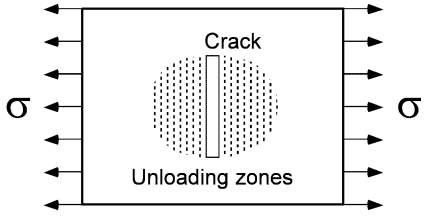

Fig. 1. Material unloading zones around the crack surface.

difficult to model complex three-dimensional cyclic response of concrete. These, as well some other drawbacks of the constitutive laws based on the theory of tensorial invariants is the main motivation for the use of the microplane theory as an alternative approach for macroscopic modeling of concrete.

2. Microplane material model

In the microplane model, the material is characterized by a relation between the stress and strain components on planes of various orientations. These planes may be imagined to represent the damage planes or weak planes in the microstructure, such as contact layers between aggregate pieces in concrete (Fig. 2). In the model, the tensorial invariance restrictions need not be directly enforced. They are automatically satisfied by superimposing in a suitable manner, the responses from all the microplanes. Basic concept behind the microplane model was advanced (G.I. Taylor, 1938) and developed in detail for plasticity (Batdorf and Budianski, 1949), under the name "slip theory of plasticity". Later, the model was extended by Bažant and co-workers for modeling of quasi-brittle materials, which exhibit softening (Bažant and Gambarova, 1984; Bažant and Prat, 1988; Bažant and Ožbolt, 1990; Carol et al., 1992; Bažant et al., 1996a,b, 1998). For hardening the materials, it was assumed that the stress vector which acts on various planes in the material (slip plane) was the projection of the macroscopic stress tensor (static constraint). To provide a unique solution for the softening materials, it was realized (Bažant, 1984) that the static constraint needed to be replaced by the kinematic constraint, where the microplane strain components are calculated as the projection of the macroscopic strain tensor.

The advanced kinematic constraint version of the model for concrete was developed by Bažant and Prat (1988) and later extended to a general cyclic form with the rate sensitivity by Ožbolt and Bažant (1992). This model has been implemented into the two- and three-dimensional nonlocal finite element code and rather broad experience has been gained with it so far. Let us first summarize some of its qualities: (i) The main advantage of the model is its conceptual simplicity i.e. only a set of uniaxial stress–strain curves on the microplane need to be defined and the macroscopic model response comes automatically out as a result of the numerical integration over a number of microplanes; (ii) the model covers full three-dimensional range of applicability; (iii) it is relatively easy to account for the initial anisotropy; (iv) the comparison between the test data and the model response for different stress–strain histories demonstrated a good agreement

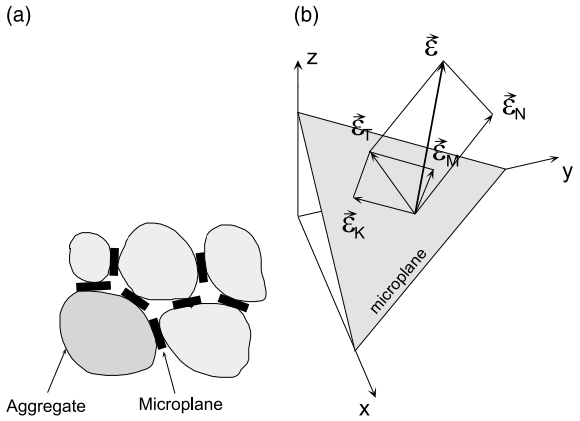

Fig. 2. Microplane model: (a) load transfer over a number of idealized contact planes and (b) decomposition of the total macroscopic strain tensor on the microplane.

(Bažant and Prat, 1988; Bažant and Ožbolt, 1990; Bažant et al., 1996a,b, 1998); (v) implementation in the finite element code and a number of numerical studies that have been carried out have indicated the capability of the model in realistic prediction of concrete behavior. However, for dominant tensile damage (tensile softening), the model exhibits pathological behavior which is manifested by unrealistic lateral expansion.

To model concrete for dominant compressive load realistically and to control the initial elastic value of Poisson's ratio, in Bažant and Prat's model, the normal microplane component is decomposed into volumetric and deviatoric part. Moreover, the deviatoric compressive strength as well as the shear strength need to be set roughly 10 times larger than the volumetric and deviatoric tensile strength. As shown by Jirásek (1993), the main reason for pathological behavior of Bažant and Prat's microplane model subjected to tension is related to the split of the normal microplane component into volumetric and deviatoric part and not to the kinematic constraint itself. To demonstrate why the problem arises only for tensile load, let us consider a specimen loaded in uniaxial tension (plane stress state, Fig. 3a). For simplicity reasons only two microplanes (x and y) are considered. Plane x is oriented in the load direction and plane y is perpendicular to it. According to Bažant and Prat's model, the normal microplane stress and strain component in the plane y ($\sigma_{N,y}$, $\varepsilon_{N,y}$) is split into volumetric (σ_V, ε_V) and deviatoric ($\sigma_{D,y}$, $\varepsilon_{D,y}$) part:

$$\varepsilon_{N,y} = \varepsilon_V + \varepsilon_{D,y}, \qquad \sigma_{N,y} = \sigma_V + \sigma_{D,y}, \tag{1a}$$

with

$$\sigma_y = \sigma_{N,y} = 0. \tag{1b}$$

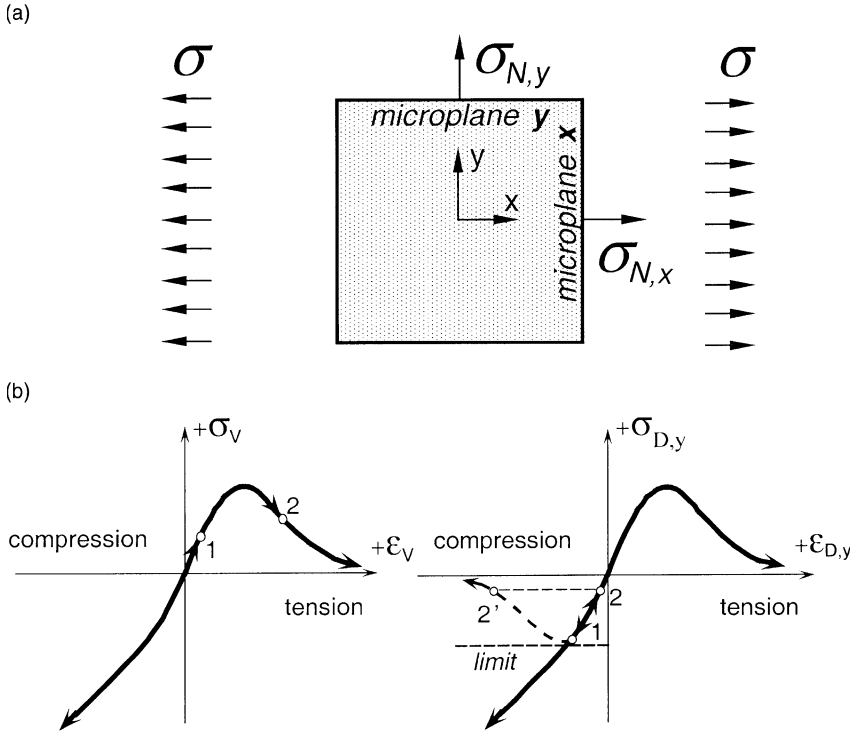

Fig. 3. Volumetric and deviatoric microplane strain components for simple two-plane microplane model: (a) microplanes loaded in uniaxial tension (plane stress) and (b) volumetric and deviatoric stress–strain components.

The volumetric and deviatoric strain component on the plane y are for the linear elastic response (approximately point 1, Fig. 3b):

$$\varepsilon_V = 1/3(1-2v)\varepsilon_x, \qquad \varepsilon_{D,y} = -1/3(1+v)\varepsilon_x, \tag{2}$$

where v is Poisson's ratio and ε_x, the total strain in the direction of the applied tensile load. From Eq. (2), it follows that for $\varepsilon_x > 0$, the deviatoric stress and strain components of plane y are negative (compression, see Fig. 3b). In the crack state the load reduces to zero ($\varepsilon_x \to +\infty;\ \sigma = \sigma_x = 0$). Consequently, the volumetric stress reduces to zero as well ($\sigma_V = 0$). From Eq. (1) is then obvious that $\sigma_{D,y} = 0$. In Bažant and Prat's model, the volumetric and deviatoric stresses for virgin loading are calculated as

$$\sigma_V = C_V\varepsilon_V, \qquad \sigma_{D,y} = C_D\varepsilon_{D,y} \tag{3}$$

in which C_V and C_D are the secant stiffness moduli for volumetric and deviatoric components, respectively. The shape of the stress–strain curves is qualitatively plotted in Fig. 3b. Using Eqs. (3) and (1a), condition (1b) is for the cracked state fulfilled either for: (I) $C_D = 0$ or for (II) $\varepsilon_{D,y} = 0$. The first implies that the deviatoric component on plane y undergoes softening (dotted line in Fig. 3b). Since in Bažant and Prat's model, for concrete, the deviatoric compressive strength is roughly 10 times greater than the volumetric tensile strength, condition (1b) is satisfied by the second condition ($\varepsilon_{D,y} = 0$), i.e. the deviatoric strain component $\varepsilon_{D,y}$ does not undergo softening. Consequently, from condition (II) and (1a), it follows that $\varepsilon_{N,y} = \varepsilon_V$ i.e. for uniaxial tensile fracture the model predicts lateral expansion.

Introducing Eq. (3) into Eq. (1) and denoting $\eta = C_{D,y}/C_V$ it follows:

$$\eta = -\varepsilon_V/\varepsilon_{D,y}. \tag{4}$$

For the linear elastic stress–strain state, η is obtained using Eq. (2) as $\eta = (1-2v)/(1+v)$. Analogous to the elastic solution, to fulfill condition (I) for cracked state, η should be constant for any level of damage, and therefore,

$$C_{D,y} = \eta C_V. \tag{5}$$

According to Eq. (5), condition (I) is fulfilled only when $C_{D,y}$ is proportional to C_V during the entire load (damage) history. Only such stress–strain relationship for deviatoric component which satisfies Eq. (5) yields the realistic solution for the uniaxial tension. If the relationship is different, the model predicts the pathological lateral expansion (condition II is satisfied) or the normal stress component $\sigma_{N,y}$ for $\varepsilon_x = +\infty$ ($\sigma_x = 0$) does not reduce exactly to zero.

One of the consequences of the pathological model response observed in the finite element analysis is illustrated by two simple examples. First, the unit plane stress finite element with four integration points is loaded in uniaxial tension. The calculated normalized stress–strain curves for axial and lateral strain components are plotted in Fig. 4a. It can be seen that before the tensile strength is reached (hardening), the material correctly contracts in the lateral direction, however, after the onset of cracking, the model predicts lateral expansion. At the end of the softening process, the lateral strain is the same as the axial strain i.e. the ratio between the axial and the lateral strain is equal to one. Second, the same element is loaded in tension and then, for a constant tensile stress lesser than the tensile strength, loaded in shear up to failure. The shear load is applied by controlling the horizontal displacements of two upper nodes of the element. The element is assumed to be unrestrained perpendicular to the direction of the applied shear load. Fig. 4b shows the calculated normalized shear stress–strain curves for different levels of tensile stresses. It can be seen that the model correctly predicts the maximum shear resistance, which decreases to zero, when the tensile stress reaches the tensile strength. However, as soon as the shear resistance is reached, the stress–strain curves exhibit unrealistic instability as a consequence of pathological expansion.

To formulate a more realistic microplane model for dominant tensile load, one has to account for discontinuity of the strain field. There are principally two different ways to do this: (1) imposing the static

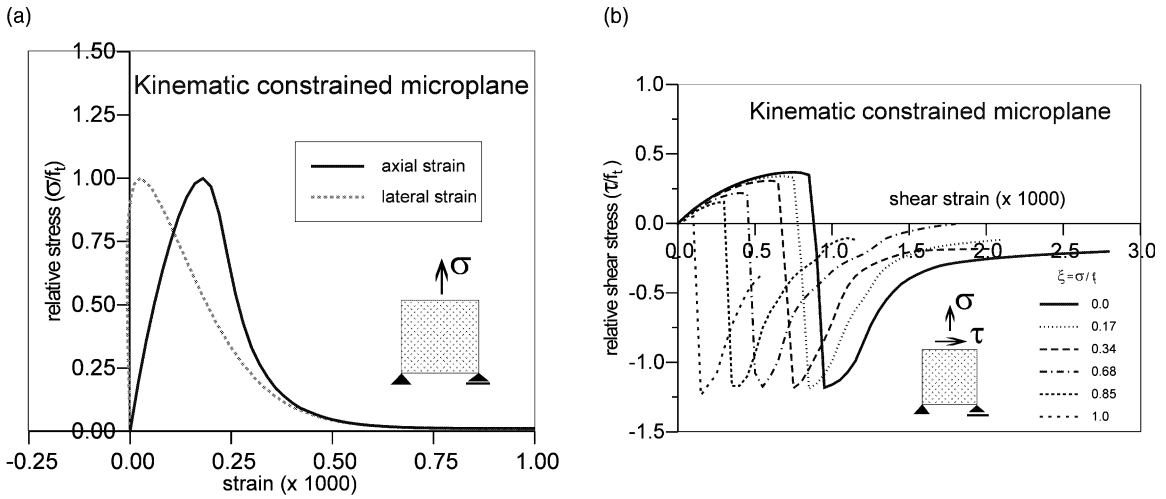

Fig. 4. Bažant and Prat's kinematic constrained microplane for dominant tensile load: (a) Axial and lateral strains for uniaxial tensile load and (b) shear stress–strain curves for different levels of tensile load.

constraint approach at the microplane level or (2) keeping the kinematic constraint approach, but modifying the microplane strain components by adopting additional constraints. The first approach would mean that the microplane stress components are calculated as the resolved components of the total macroscopic stress tensor. Because of the non-unique definition of the stress tensor in softening materials, as mentioned above, it is generally difficult to work directly with the static constraint approach. Therefore, the kinematic constraint approach should be improved.

To improve the model, Bažant et al. (1996a,b) proposed the microplane model with "stress–strain boundaries" in which split/no split of normal microplane components is not fixed a priori, but decided for each microplane individually depending on the current strain. The model basically eliminates the pathological behavior; however, as shown by Jirásek (1998), for uniaxial tension, the stress does not generally reduce exactly to zero. In the model, the microplane components have stress limits (strengths) which are generally a function of the macroscopic stress tensor. Since no explicit relation between these strengths and macroscopic stress tensor exists, for general loading–unloading histories, a skip from one stress limit to the other can occur. This may be a source of numerical difficulties when the model is used in a general finite element code. Furthermore, Carol and Bažant (1995) proposed a plasticity type of decomposition of macroscopic strains, in which the "plastic" part has the meaning of crack opening and "elastic" part goes into microplanes. The same authors also proposed a microplane formulation in which the concept of damage and plasticity were introduced at the microplane level. The relations for the macroscopic plastic strains and damage tensors are obtained as integrals of their microplane counterparts (Carol and Bažant, 1997). The plastic part of the model was formulated with split of normal components, while the damage part was formulated without split. Loading surfaces and flow rules were defined at microplane level, and macroscopic counterparts could also be obtained under certain conditions. Although these approaches results in a physically correct model response, the conceptual simplicity of the kinematic constraint model is lost. Instead of a simple uniaxial stress–strain law for each microplane, integral stress–strain dependency is needed, and cyclic modeling appears to become more difficult.

To eliminate pathological behavior of the microplane model, in the present paper, an alternative approach is proposed. In the proposed model, which is principally based on the model of Bažant and Prat (1988) and Ožbolt and Bažant (1992), the loss of continuity of the strain field for dominant tensile load is at the microplane level accounted for by adopting the so-called effective microplane strain components. The

components are calculated such that Eq. (5) is approximately fulfilled for the entire tensile load history. Furthermore, the initial material anisotropy for possible modeling of fiber reinforced concrete is introduced as well. The model is tested on the material and structural levels for different monotonic and cyclic load histories and the results are compared with the available test evidence.

3. Microplane model with relaxed kinematic constraint

3.1. Basic assumptions and macro–micro relationships

To keep the conceptual simplicity of the improved model, most of the assumptions originally introduced by Bažant and Prat (1988) and Ožbolt and Bažant (1992) are kept the same. However, instead of working with the microplane strain calculated from the total strain tensor (continuous strain field), for dominant tensile load the microplane stress is calculated from the effective microplane strain. The main assumptions are as follows:

(I) Each microplane resists normal and shear strain components (ε_N, ε_T). The normal strain component is decomposed into volumetric (ε_V) and deviatoric part (ε_D). The resulting shear consists of two mutually perpendicular components (ε_M, ε_K) (Fig. 2b).

(II) Except for volumetric strain, the effective microplane strains are resolved components of the total macroscopic strain tensor ε_{ij} multiplied by function ψ:

$$\vec{\varepsilon}_N = (\varepsilon_D + \varepsilon_V)\vec{n}, \qquad \varepsilon_V = \varepsilon_{kk}/3, \qquad \varepsilon_D = (n_i n_j \varepsilon_{ij} - \varepsilon_V)\psi, \tag{6a}$$

$$\vec{\varepsilon}_T = \varepsilon_M \vec{m} + \varepsilon_K \vec{k}, \qquad \varepsilon_M = m_i n_j \varepsilon_{ij}\psi, \qquad \varepsilon_K = k_i n_j \varepsilon_{ij}\psi. \tag{6b}$$

The orientation of each microplane in Eq. (6) is characterized by the unit normal **n** of components n_i where i represents the components of the Cartesian coordinates x_i (i = 1, 2, 3).

(III) For dominant tensile load function, ψ introduced in Eq. (6) relaxes the kinematic constraint. It reflects discontinuity as a consequence of discrete tensile cracking, therefore, we call this function *discontinuity function*. It is for each microplane individually decided whether the function applies ($1 \geqslant \psi \geqslant 0$) or not. The discontinuity function ψ is not chosen arbitrarily. As will be discussed later, for individual microplanes, ψ is related to the volumetric stress–strain relationship. In addition, to account for a smooth transition from dominant tensile to dominant compressive load, the function is also assumed to be dependent on the maximum principal stress σ_I (tension).

(IV) For correct modeling of concrete at high confining pressures, the shear response on each microplane is assumed to be dependent on the volumetric strain. The microplane shear components are mutually independent. Consequently, there is no co-axiality between their stress and strain components.

From known microplane strain increments, the corresponding microplane stresses are calculated as

$$\begin{aligned} d\sigma_V &= E_V d\varepsilon_V, \qquad d\sigma_D = E_D d\varepsilon_D, \\ d\sigma_M &= E_M d\varepsilon_M, \qquad d\sigma_K = E_K d\varepsilon_K, \end{aligned} \tag{7a}$$

where E_V, E_D, E_M, E_K represent tangent moduli obtained from known uniaxial microplane stress–strain relationships. In the present model, the relationships for virgin loading are adopted the same as proposed by Ožbolt and Bažant (1992). They are based on the scalar damage theory and are as follows:

$$\sigma_V = C_V \varepsilon_V, \quad \sigma_D = C_D \varepsilon_D, \quad \sigma_T = C_T \varepsilon_T \tag{7b}$$

with (except for volumetric compression):

$$C_V = E_{V,0}(1 - \omega_V), \qquad C_D = E_{D,0}(1 - \omega_D), \qquad C_T = E_{T,0}(1 - \omega_T), \tag{7c}$$

where C_V, C_D and C_T are secant moduli with their initial values $C_{V,0} = E_{V,0}, C_{D,0} = E_{D,0}$ and $C_{T,0} = E_{T,0}$. The shear microplane moduli C_T denotes both components M and K. They are assumed to have the same function. Scalar damage parameters ω are adopted as:

$$\begin{aligned} &\varepsilon_V \geqslant 0: \ \omega_V = 1 - e^{-|\varepsilon_V/e_1|^m}, \\ &\varepsilon_D \geqslant 0: \ \omega_D = 1 - e^{-|\varepsilon_D/e_1|^m}, \quad \varepsilon_D < 0: \ \omega_D = 1 - e^{-|\varepsilon_D/e_2|^n}, \\ &\omega_T = 1 - e^{-|\varepsilon_T/e_5|^k} \end{aligned} \tag{7d}$$

in which $e_5 = e_3$ when $\varepsilon_V \geqslant 0$ and $e_5 = e_3 - e_4\varepsilon_V$ if $\varepsilon_V < 0$. Parameters e_1, e_2, e_3, e_4, m, n and k are empirical material constants. The dependence of e_5 on the volumetric strain ε_V reflects internal friction which is an additional kinematic constraint of a scalar type. For volumetric compression, there is no damage ($\omega_V = 0$), therefore, the stress–strain relationship is adopted as

$$C_V = E_{V,0}\left[\left(1 + \left|\frac{\varepsilon_V}{a}\right|\right)^{-p} + \left|\frac{\varepsilon_V}{b}\right|^q\right], \tag{7e}$$

where a, b, p, q are again empirical constants. Note that one could also use another set of microplane curves which can reproduce the behavior of concrete on the macro scale well. The curves from Eq. (7) for all microplane stress–strain components are schematically plotted in Fig. 5. As can be seen, in contrast to volumetric and deviatoric components, the shear component is assumed to be symmetric.

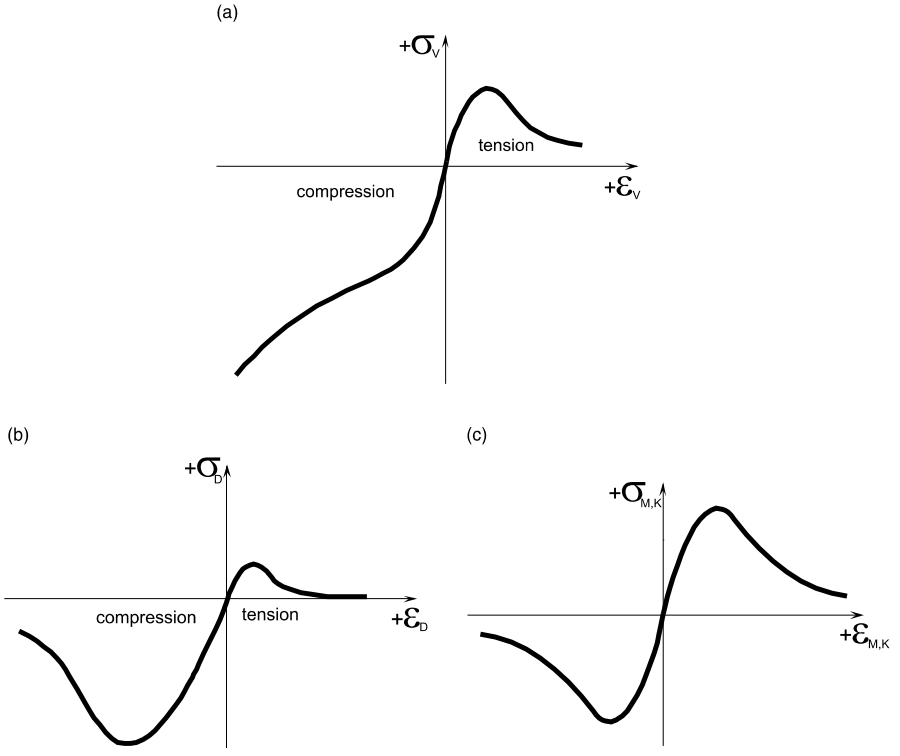

Fig. 5. Schematic plot of microplane stress–strain relationships for virgin load: (a) volumetric component (V), (b) deviatoric component (D) and (c) shear stress–strain components (M and K).

To generate the macroscopic stiffness and stress tensor from known microplane stress and strain components, one has to integrate the uniaxial stress–strain laws over all the microplanes such that the stress equilibrium between all the microplane stresses and macroscopic stress tensor is approximately fulfilled (Ožbolt and Bažant, 1992). Due to the material nonlinearity and path dependency (cyclic loading), this has to be done incrementally. The microplane stress increments are calculated from stress–strain relationships (7). From these increments, the corresponding macroscopic stresses are obtained by imposing equilibrium between macro and micro level. In the total form, the equilibrium can approximately be enforced by the virtual work equation (Bažant and Prat, 1988) as

$$\frac{2\pi}{3}\sigma_{ij}\delta\varepsilon_{ij} = \int_S (\sigma_N\delta\varepsilon_N + \sigma_M\delta\varepsilon_M + \sigma_K\delta\varepsilon_K)\Omega(\mathbf{n})\mathrm{d}S, \tag{8}$$

where $\mathbf{n}$ represents unit vectors normal to the microplanes. $\delta\varepsilon_{ij}$, $\delta\varepsilon_N$, $\delta\varepsilon_M$, $\delta\varepsilon_K$ are small variations of the strains on the macro and microlevels. The left-hand side of Eq. (8) represents the macroscopic work done on the unit sphere of the material while the right-hand side represents the macroscopic work done over the surface of the same sphere. $\delta\varepsilon$ contains small variation of the strains due to microcracking (damage) as well as the variation of strains due to frictional plastic slip. $\Omega(\mathbf{n})$ is a weight function of the normal direction $\mathbf{n}$ that introduces anisotropy of the material in its initial state. For normal concrete we assume $\Omega(\mathbf{n}) = 1$, which implies initial isotropy. As will be discussed later, for some materials (fiber reinforced concrete) we may also account for the initial anisotropy. Substituting assumption (6) into Eq. (8) we get the macroscopic stress tensor as

$$\sigma_{ij} = \frac{3}{2\pi}\int_S \left[n_i n_j\sigma_V + n_i n_j\sigma_D + \frac{1}{2}(m_i n_j + m_j n_i)\sigma_M + \frac{1}{2}(k_i n_j + k_j n_i)\sigma_K\right]\Omega(\mathbf{n})\mathrm{d}S. \tag{9}$$

The integral in Eq. (9) is linear in stress and therefore it applies on the stress increments as well.

It has been recently pointed out by Carol and Bažant (1997) that the term $(n_i n_j)$ which in Eq. (9) stays with σ_D should actually be replaced by $(n_i n_j - \delta_{ij}/3)$ i.e. $-\delta_{ij}/3$ should be added. As shown by Bažant et al. (1998), the term has no effect on the elastic response, however, it can have an effect on the inelastic response. The stronger the difference in the tensile and compressive deviatoric strengths, the greater will be the effect of the term $-\delta_{ij}/3$. The absence of the term can cause violations of thermodynamic restrictions, particularly negative dissipation during a closed strain cycle (Bažant et al., 1998). In the present model the absence of the term $-\delta_{ij}/3$ is compensated by adopting the ratio between initial deviatoric and volumetric modulus to be less than one ($\eta = E_{D,0}/E_{V,0} < 1$) as well as taking the shear microplane strength as greater than the deviatoric compressive strength. Moreover, the effect is also compensated by the dependency of the microplane shear resistance on the volumetric strain as well as by the discontinuity function, which, the deviatoric and shear strain makes dependent on the total volumetric strain.

The kinematic constraint approach a priori assumes continuity of the strain field i.e. small variations of the macroscopic strain field ($\delta\varepsilon_{ij}$), in the sense of the smeared crack approach, are proportional to the small variation of the microplane strain components ($\delta\varepsilon_N$, $\delta\varepsilon_M$, $\delta\varepsilon_K$). However, as soon as strain localization and cracking (discontinuity) occurs, variation of the macroscopic strains is not proportional to the variation of the microplane strains. This is schematically plotted in Fig. 6 and it is in the present formulation accounted for through the effective microplane strains.

The same, as shown by Ožbolt and Bažant (1992), macroscopic tangent material stiffness tensor E_{ijrs} is obtained by substituting Eq. (6) and incremental form of Eqs. (7b)–(7e) into the incremental form of Eq. (9),

$$E_{ijrs} = \frac{3}{2\pi}\int_S \left[n_i n_j n_r n_s E_D + \frac{1}{3}n_i n_j\delta_{rs}(E_V - E_D) + \frac{1}{4}(m_i n_j + m_j n_i)(m_r n_s + m_s n_r)E_M + \frac{1}{4}(k_i n_j + k_j n_i)(k_r n_s + k_s n_r)E_K\right]\Omega(\mathbf{n})\mathrm{d}S, \tag{10}$$

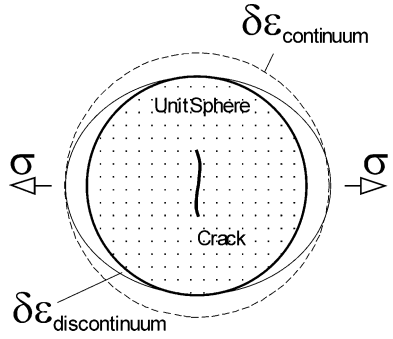

Fig. 6. Virtual strain field – continuum and discontinuum.

where E_V, E_D, E_M and E_K are tangent moduli of the corresponding microplane components. The integrals from Eqs. (9) and (10) are evaluated numerically employing the following approximate formula:

$$\frac{4\pi}{3}\int_S \cong 6\sum_{\kappa=1}^{n} X_\kappa \tag{11}$$

in which subscript κ refers to a certain discrete set of microplanes characterized by the spatial discretization of their normals associated with points on a unit hemisphere, and X_κ are the weights (numerical integration coefficients) for these directions. The meaning of Eq. (11) is that the unit sphere from Eq. (8) is approximated by a number of discrete planes (Fig. 7). According to the present experience, 21-point integration formula (Bažant and Oh, 1986) gives sufficient accuracy. The numerical algorithm to calculate macroscopic stress tensor σ_{ij} from known microplane stresses is the same as described by Ožbolt and Bažant (1992).

3.2. Relaxation of the kinematic constraint for tensile load

At a lower tensile load, concrete can be viewed as an isotropic elastic continuum. With increase of load, in the weak zone, a band of microcracks forms which by subsequent loading coalesce into a crack i.e. debonding of the material particles (rupture) takes place. In the framework of the continuum theory, cracking is represented by the localization of strains. When the strain increases, the stress oriented in the same direction (damage direction, direction 1 in Fig. 8) decreases. The strain components which are oriented predominantly laterally to the direction of damage (direction 2 in Fig. 8) decrease approximately elastically i.e. after the damage evolution is completed (rupture), the three-dimensional stress–strain state at

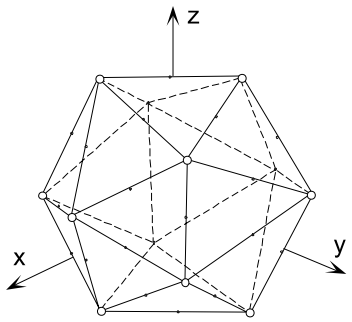

Fig. 7. Spatial discretization (approximation) of the sphere by 21 integration points (symmetric part).

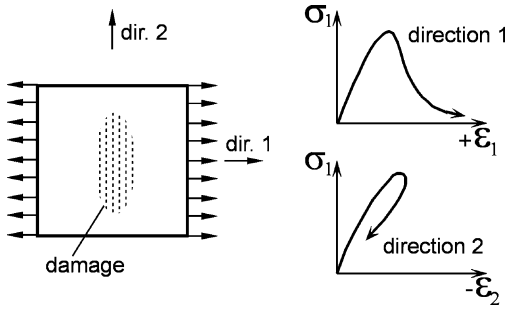

Fig. 8. Macroscopic loading–unloading of the material as a function of the damage orientation.

the beginning of loading shrinks into a uniaxial stress–strain state. This effect is essentially a structural effect which should be accounted for in any macroscopic material model. The micromechanical models account for this effect automatically.

Before we decide how to calculate the effective microplane strains (assumption III), we have to choose an objective criterion for dominant tensile load. For direct tension in one, two or in all three directions, compression-tension, unrestricted shear (no restrains perpendicular to the shear direction) with or without tension, the volumetric strain as well as maximum principal stress are positive. Therefore, it is reasonable to assume that the dominant tensile load exists when

$$\varepsilon_V > 0 \quad \text{and} \quad \sigma_I > 0, \tag{12}$$

where σ_I is the maximum principal stress. Both quantities (ε_V, σ_I) are invariant macroscopic properties. In the linear elastic range, principal stress controls the existence of tensile load. For a fully cracked specimen, the total volumetric strain is positive and the principal stress is close to zero. In the sense of the smeared crack approach, strains in the direction of tensile load are large and those perpendicular to it are practically zero (unloading) i.e. the resulting volumetric strain is positive. Moreover, the total volumetric strain in cracked material is approximately the same as the nonelastic ('plastic') volumetric strain and, therefore, it can be used as an indicator of tensile damage.

Unlike the models proposed by Carol and Bažant (1995, 1997), the use of the effective strains introduced in Eq. (6) is not motivated by the theory of plasticity. Namely, the same as in the plasticity, the total microplane strain component ε_{mp} can formally be decomposed into nonelastic (relaxed) part $\varepsilon_{mp,r}$ and the stress effective part $\varepsilon_{mp,eff}$:

$$\varepsilon_{mp} = \varepsilon_{mp,r} + \varepsilon_{mp,eff}, \qquad \varepsilon_{mp,eff} = \varepsilon_{mp}\psi, \tag{13}$$

where mp denotes the corresponding microplane component (D, M, K). The actual motivation for the use of discontinuity function are physical arguments discussed above and Eq. (5) which is related to a simple two-plane microplane model discussed in Section 2. According to Eq. (5), the deviatoric secant moduli C_D should be for the entire tensile load history proportional to the volumetric secant moduli C_V. Using (5) and the microplane stress–strain relationships (7), the deviatoric microplane stress component for virgin load is calculated as

$$\sigma_D = C_D \varepsilon_D e^{-|\varepsilon_V/e_1|^m}, \tag{14}$$

where ε_D denotes total deviatoric strain. Eq. (14) can be rewritten as

$$\begin{aligned} &\sigma_D = C_D \varepsilon_{D,eff} \quad \text{or} \quad \sigma_D = C_{D,eff}\varepsilon_D, \\ &\varepsilon_{D,eff} = \varepsilon_D \psi, \quad C_{D,eff} = C_D \psi \ \text{ with } \psi = e^{-|\varepsilon_V/e_1|^m}, \end{aligned} \tag{15}$$

where $C_{D,eff}$ can be interpreted as an effective secant moduli chosen such that Eq. (5) holds. According to Eq. (15), for virgin loading, the deviatoric stresses can formally be calculated by the use of the effective strains or alternatively using total deviatoric strains ε_D multiplied by the effective secant deviatoric moduli $C_{D,eff}$, which varies from $C_{D,0}$ (initial state) to 0 (crack state) and is proportional to C_V. In both cases the final result is the same i.e. η remains constant for the entire tensile load history what prevents pathological model response. The discontinuity function ψ has to be of the same type as a function which controls the volumetric secant modulus C_V Eq. (7c). If we would use an arbitrary function, the pathological behavior could be eliminated, however, the macroscopic tensile stresses at crack state would generally not reduce to zero.

Analogous to the deviatoric component, the same discontinuity function is used for microplane shear components. Practical effect of the discontinuity function for deviatoric and shear components is relaxation of the material in the direction perpendicular to the principal damage direction. This agrees with the physical arguments discussed at the beginning of this section. By replacing the total deviatoric strain component with the effective one, the final result is similar to that for the model with the concept of stress boundaries (limit stress, Fig. 3b) proposed by Bažant et al. (1996a,b).

To account for the orientation of tensile dominant damage (crack orientation) the activation of discontinuity function on the individual microplanes is controlled by the deviatoric microplane strain component. As demonstrated in Section 2, at the onset of cracking (localization of strain), the microplane which is perpendicular to the crack surface has negative deviatoric strain ($\varepsilon_D = \varepsilon_N - \varepsilon_V;\ \varepsilon_N \to 0$ and $\varepsilon < 0$) i.e. the plane need to be unloaded (relaxed). On the contrary, the microplane which is parallel to the crack surface, has positive deviatoric strain ($\varepsilon_D = \varepsilon_N - \varepsilon_V;\ \varepsilon_N > \varepsilon_V;\ \varepsilon_N > 0 \to \varepsilon_D > 0$) and it is loaded in tension. Consequently, depending on whether the microplane is loaded or unloaded, the total strain for individual deviatoric and shear components need not or need be multiplied by discontinuity function.

3.2.1. Discontinuity function for the normal microplane strain component

According to Eq. (6), the normal microplane strain component is decomposed into volumetric and deviatoric part. Although the volumetric strain component for individual microplanes could principally be split into the effective and noneffective part, because of the following reasons the volumetric strain is not split: (1) the volumetric strain is invariant with respect to the microplane orientation, (2) the static constraint on volumetric stress for tensile load is automatically fulfilled ($\varepsilon_V \to +\infty, \sigma_V \to 0$), (3) it serves as a macroscopic indicator for tensile dominant damage and (4) in the total (not decomposed) form, it is useful for monitoring of the stress–strain path of concrete under tensile cyclic loading.

As discussed above, negative deviatoric strain component means that the microplane normal is oriented close to the direction which is orthogonal to the damage direction. Therefore, when damage increases the deviatoric microplane stress and strain components for these directions should approximately relax (unload) to zero. To account for the above effect, the discontinuity function for the deviatoric strain is taken as

$$\varepsilon_D < 0,\ \ \varepsilon_V > 0,\ \ \sigma_I > \sigma_{I,min} \quad \psi = e^{-|f(\sigma_I)\varepsilon_V/e_1|^m}, \tag{16a}$$

$$\varepsilon_D \geqslant 0 \quad \psi = 1. \tag{16b}$$

The discontinuity function in Eq. (16a) is taken as discussed before, i.e. it has principally the same shape as the microplane stress–strain relationship for volumetric tension. Function $f(\sigma_I)$ in Eq. (16a) (Fig. 9) is introduced to assure a smooth transition from discontinuous state (tensile crack) into continuous state (crack closure and subsequently loading in compression). Based on the fit of the cyclic test data, the function is adopted as

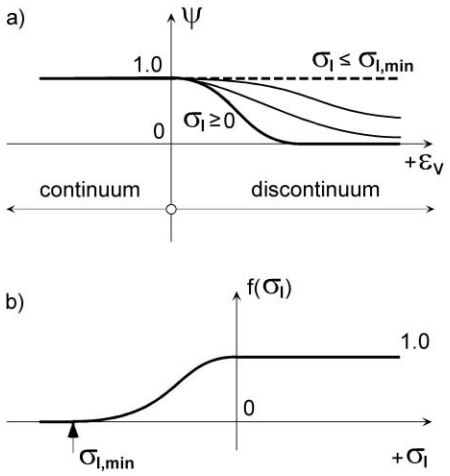

Fig. 9. Discontinuity criterion: (a) Strain discontinuity function and (b) stress discontinuity function.

$$\begin{aligned}
&\sigma_{\mathrm{I,min}} \leqslant \sigma_{\mathrm{I}} \leqslant 0: \quad f(\sigma_{\mathrm{I}}) = 1 - \chi, \quad \chi = \sin\left(\frac{\pi}{2}\left|\frac{\sigma_{\mathrm{I}}}{\sigma_{\mathrm{I,min}}}\right|\right),\\
&\sigma_{\mathrm{I}} > 0: \quad f(\sigma_{\mathrm{I}}) = 1,\\
&\sigma_{\mathrm{I}} < \sigma_{\mathrm{I,min}}: \quad f(\sigma_{\mathrm{I}}) = 0
\end{aligned} \tag{17}$$

in which $\sigma_{\mathrm{I,min}}$ is a small negative limit value of the maximum principal stress.

For the planes which are oriented predominantly in the damage direction ($\varepsilon_{\mathrm{D}} > 0$), total strain perpendicular to the crack surface yields infinity and the corresponding stress reduces to zero. Consequently, for these microplanes $\varepsilon_{\mathrm{V}} \to +\infty$, σ_{V}, σ_{D}, $\sigma_{\mathrm{T}} \to 0$ and $\varepsilon_{\mathrm{D}} \to +\infty$ with $\psi = 1$.

3.2.2. Discontinuity function for the shear microplane strain components

The microplane shear resistance depends on the normal microplane stresses. For positive normal stress (tension), after the onset of cracking, the shear resistance reduces to zero. On the contrary, for negative normal stress (compression), the microplane offers resistance over shear softening regime mainly through friction and it generally does not reduce to zero. Typical situation when this occurs is compression or shear-compression softening where microplane shear resistance predominantly relies on shear-friction due to the effect of normal compressive stresses. For these stress–strain states concrete is modeled as a cracked continuum. However, for dominant tensile damage, independent of the microplane orientation, the shear strain and stress components relax to zero. Consequently, the shear discontinuity function for individual microplanes are

$$\varepsilon_{\mathrm{V}} > 0, \quad \sigma_{\mathrm{I}} > \sigma_{\mathrm{I,min}} \quad \psi = \mathrm{e}^{-|f(\sigma_{\mathrm{I}})\varepsilon_{\mathrm{V}}/e_1|^m} \tag{18a}$$

$$\text{else}: \quad \psi = 1. \tag{18b}$$

As discussed before, function (18) is the same as the one for the deviatoric component in Eq. (16).

The discontinuity function for microplane shear stress component plays an important role by modeling of shear failure. When shear fracture is modeled by the three-invariant plasticity based models for concrete (Willam et al., 1999), the shear damage unrealistically spreads over a few elements. On the contrary, in the present microplane model ψ enables localization of damage in a row of single finite elements. Consequently,

smeared fracture modeling of concrete becomes closer to the discrete crack approach and therefore more realistic.

3.3. Unloading, reloading and cyclic loading

To model unloading, reloading and cyclic loading for general triaxial stress–strain states, loading–unloading rules for each microplane stress–strain component are introduced. In the present model, these rules are a simplification of the rules introduced by Ožbolt and Bažant (1992).

The virgin loading for each microplane strain component occurs if

$$\varepsilon\Delta\varepsilon \geqslant 0 \quad \text{and} \quad (\varepsilon - \varepsilon_{\max})(\varepsilon - \varepsilon_{\min}) \geqslant 0, \tag{19}$$

where $\varepsilon_{\max}$ and $\varepsilon_{\min}$ are the maximum and minimum values of the effective microplane strain that have occurred so far; otherwise unloading or reloading takes place. In contrast to virgin loading, for cyclic loading the stress–strain relations must be written in the incremental form:

$$\mathrm{d}\sigma = E\mathrm{d}\varepsilon, \tag{20}$$

where E represents unloading–reloading tangent moduli which is generally defined as

$$\begin{aligned} &E = E_0\alpha + \sigma\left(\frac{1-\alpha}{\varepsilon - \varepsilon_1}\right), \\ &\varepsilon > \varepsilon_p, \quad \varepsilon_1 = \varepsilon_p - \frac{\sigma_p}{E_0} + \beta(\varepsilon - \varepsilon_p), \\ &\varepsilon \leqslant \varepsilon_p, \quad \varepsilon_1 = 0. \end{aligned} \tag{21}$$

In Eq. (21), σ_p and ε_p denote the positive or negative peak stress and the corresponding strain for each microplane component using values σ_{p^+}, ε_{p^+} and σ_{p^-}, ε_{p^-} for positive and negative peaks, α and β are empirically chosen constants between 1 and 0 and E_0 is initial elastic stiffness moduli for the corresponding microplane component.

The loading–unloading–reloading rules for microplane components are schematically plotted in Fig. 10. Fig. 10a shows cyclic rules of the volumetric stress–strain component. In the compressive part the loading–

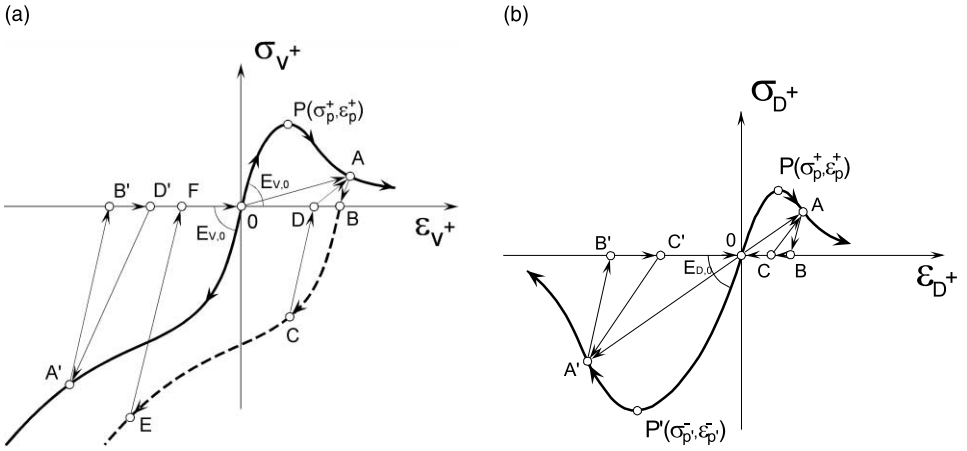

Fig. 10. Loading–unloading and reloading rules for microplane strain components: (a) Volumetric component and (b) deviatoric component.

unloading modulus is defined by the initial elastic modulus $E_{V,0}$. For tension the unloading and reloading moduli are controlled by Eq. (21). Typical load cycle for virgin loading in tension, unloading in compression and reloading in tension is O–P–A–B–C–D–A–B–E–F–O–A. Virgin loading in compression, unloading and subsequent loading in tension follows the path: O–A′–B′–D′–A′ or O–A′–B′–O–P–A–B–E–F–O–A. For the deviatoric compression and tension similar rules as those for the volumetric tension are employed (Fig. 10b). The loading–unloading–reloading rules for shear are principally the same as for the deviatoric component.

From the bond cyclic experimental evidence, in which the shear damage plays an important role, it is known that loading in one direction causes damage which is manifested by degradation of shear strength and stiffness in the opposite direction (Eligehausen et al., 1983; Balazs, 1991). To account for this effect, the shear microplane component is modified such that the microplane shear stiffness moduli E_M and E_K are multiplied by an additional damage function:

$$\omega_S = e^{-1.2(\Lambda/\Lambda_0)^{1.1}}, \tag{22}$$

where Λ represents accumulated microplane shear energy dissipation and Λ_0 is a constant representing the area under the monotonic (undamaged) microplane shear stress–strain curve. The above equation has been proposed by Eligehausen et al. (1983) and it is based on a large number of cyclic bond test data.

The response curves, shown later in the numerical examples, provide justification of the foregoing cyclic rules. The fact that the general three-dimensional cyclic response results from simple one-dimensional cyclic rules is an important feature of the microplane material model. These relatively simple rules help us to understand better the macroscopic material response and to correlate them with the material structure and macroscopic stress and strain tensor.

3.4. Anisotropy

Generally, two kinds of anisotropy exist: (1) Initial anisotropy and (2) damage induced anisotropy. The initial anisotropy is a consequence of the material structure, i.e. by nature, the material has different properties in different directions. Damage induced anisotropy is a consequence of damage localization in a particular direction and it is a consequence of loading. In the microplane model damage induced anisotropy is automatically taken into account through the microplane stress–strain dependent constitutive laws. To account for the initial anisotropy there are two possibilities. The first, a relatively simple one, is setting function $\Omega(\mathbf{n})$ in Eq. (8) to be dependent on the orientation of the normal of each microplane relative to the given weak direction $\mathbf{w}$ (Fig. 11). From the statistical point of view, it represents a distribution function of the frequency of the directions associated with the microplane normal $\mathbf{n}$. When the microplane direction coincide with the weak, direction $\Omega(\mathbf{n}) = 1$ and if it is perpendicular to it $\Omega(\mathbf{n}) = 0$. Once the function is known, the anisotropy is automatically taken into account by introducing $\Omega(\mathbf{n})$ into Eq. (9). Since the volumetric stress is independent of the microplane orientation (volumetric isotropy) Eq. (9) is rewritten as

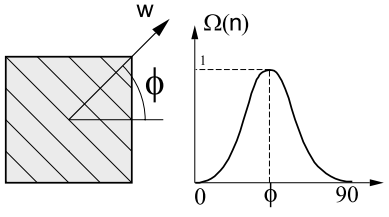

Fig. 11. Initial anisotropy – weak direction defined by angle ϕ.

$$\sigma_{ij} = \sigma_V \delta_{ij} + \frac{3}{2\pi}\int_S \left[(n_i n_j \sigma_D + \frac{1}{2}(m_i n_j + m_j n_i)\sigma_M + \frac{1}{2}(k_i n_j + k_j n_i)\sigma_K \right] \Omega(\mathbf{n}) \mathrm{d}S$$
$$\sigma_{ij} = \sigma_{ij,V} + \sigma_{ij,D}. \tag{23}$$

This method has been used for modeling of clay anisotropy (Bažant and Prat, 1987) and it is also implemented in the present microplane model. As pointed out by Bažant and Prat (1987), the main difficulty is to identify $\Omega(\mathbf{n})$ which has to be obtained from experiments. In the present model, the following empirical function is adopted:

$$\Omega(\mathbf{n}) = (n_i w_i)^{\gamma}, \tag{24}$$

where n_i stands for the components of the microplane normal $\mathbf{n}$, w_i are given components of the weak direction $\mathbf{w}$ and γ is a parameter $\geqslant 1$.

The second, more general possibility (Prat and Gens, 1994) takes advantage of the microplane formulation in which the uniaxial constitutive laws are defined for each plane of different orientation. The material anisotropy results automatically when these laws are adopted as a function of the microplane orientation. Therefore, the tangent moduli from (7a) have to be rewritten as

$$E_V = E_V(\varepsilon_V, \mathbf{n}), \qquad E_D = E_D(\varepsilon_D, \varepsilon_V, \mathbf{n}),$$
$$E_M = E_M(\varepsilon_M, \varepsilon_V, \sigma_V, \mathbf{n}), \qquad E_K = E_K(\varepsilon_K, \varepsilon_V, \sigma_V, \mathbf{n}). \tag{25}$$

The procedure to calculate the material macroscopic relations is the same as that described before. Note that in this formulation, the volumetric stress on each microplane is not the same i.e. the volumetric anisotropy is assumed.

As shown by Prat and Gens (1994), both the above discussed approaches offer a number of different possibilities for modeling material anisotropy, not only for the nonlinear material behavior, but for modeling elastic anisotropy as well. For instance, with $E_V = E_{V,0}(\mathbf{n})$, $E_D = E_{D,0}(\mathbf{n})$, $E_M = E_{M,0}(\mathbf{n})$ and $E_K = E_{K,0}(\mathbf{n})$, the elastic anisotropy can analytically be expressed by introducing these explicit relations into Eq. (10).

In the present paper, it is discussed how the initial anisotropy is introduced into the model. The implemented anisotropy will be discussed in more details in a separate paper. Therefore, the calibration as well as numerical examples related to the initial anisotropy are out of the scope of the present paper.

3.5. Material parameters and Poisson's ratio

The relation between macro and micromodel parameters at initial elastic stage is obtained by matching Eq. (8) with Hook's law (Bažant and Prat, 1988) which leads to Young's modulus (Y) and Poisson's ratio (v):

$$Y = (1-2v)E_{V,0}, \qquad v = \frac{5-2\eta-3\xi}{10+2\eta+3\xi}, \qquad \eta = \frac{E_{D,0}}{E_{V,0}}, \qquad \xi = \frac{E_{T,0}}{E_{V,0}}. \tag{26}$$

After inverting these relations, it follows that

$$E_{T,0} = \frac{1}{3}\left(\frac{5(1-2v)}{1+v} - 2\eta\right)E_{V,0}. \tag{27}$$

The above relations are obtained assuming initial isotropy. The same can be obtained for initial anisotropy. For more details see Prat and Gens (1994).

By fitting test data, it is convenient to use known (measured) values of Y (Young's modulus) and v (Poisson's ratio) as basic material parameters. The value of the ratio $\eta = E_{D,0}/E_{V,0}$ can be chosen as any real

positive value between 0 and 1 (Bažant and Prat, 1988). Later, however, it was shown that there is some preferred value, $\eta = (1 - 2v)/(1 + v)$, giving special properties with respect to the formulation of damage tensors (Carol et al., 1991; Carol and Bažant, 1997). This value is actually the same as the one obtained for simple two-plane linear elastic microplane model loaded in uniaxial tension (Section 2). The value is optimal for dominant tensile damage; however, wide experience with the use of the model indicates $\eta = 0.8$ to be optimum for most cases.

Initial Poisson's ratio and Young's modulus for concrete are known in advance. The model parameters (a, b, p, q, e_1, e_2, e_3, e_4, e_5, m, n, k) are the same as adopted in Ožbolt and Bažant (1992). For normal concrete, most of the parameters can be set as constant values and only few of them have to be obtained by fitting uniaxial compression and uniaxial tension test data. Poisson's ratio v satisfies the well-known thermodynamic restriction, namely $-1 < v < 0.5$. This follows from Eq. (19), where for $\eta \to 0$ and $\xi \to 0$, $v \to 0.5$. For $\eta \to \infty$ or $\xi \to \infty$ or both, $v \to -1$ i.e. the present microplane model for initial elastic state (no damage) covers the entire range of v. For cyclic modeling, two additional parameters α and β, the same for all microplanes, are introduced in Eq. (21). Their optimal values are obtained by fitting a set of cyclic test data (uniaxial tension, uniaxial compression and shear). According to the present experience with normal concrete, both parameters may be taken to be the same and constant for all concrete types.

To make use of the model in practical finite-element applications more comfortable, a special computer program is written, which, for basic macroscopic concrete properties (Young's modulus Y, Poisson's ratio v, uniaxial tensile strength f_t, uniaxial compressive strength f_c, concrete fracture energy G_F and concrete compressive fracture energy G_C) automatically generates the microplane model parameters.

4. Verification of the model

To verify the material model for concrete, one has to compare experimental results with the model response. Due to the fact that each test specimen is a structure which possibly exhibits size effect on the peak load and post-peak response, the calibration and verification of the macroscopic material models for quasi-brittle materials is difficult. On the macroscale, cracking phenomena are not a point but a volume property. Consequently, when the model response is compared with the test data, the model parameters need to be related to the characteristic material volume and the material properties should be filter-out from the test data. Otherwise, the model calibration is meaningless. Therefore, depending on the problem type it is not always sufficient to compare only the constitutive law with the test data since in the tests, the structural effects could possibly be significant.

The present model was recently implemented into the two- and three-dimensional finite element code and it has been so far used in a number of structural applications. To prevent spurious mesh sensitivity in the finite element calculations, the model was coupled with the regularization procedure of local (crack band) and nonlocal type. Two- and three-dimensional analysis of concrete and reinforced concrete structures were performed for problems such as: tension failure, compression and shear failure, beam-column connections (monotonic and cyclic load), splitting failure, anchor pull-out, punching and other. The discussion of these results is out of the scope of the present paper, therefore, for more details refer: Ožbolt, 1995; Ožbolt et al. 1997, 1998, 1999a,b, 2000; Eligehausen and Ožbolt, 1998; Li et al., 1998.

4.1. Effect of discontinuity function and stress locking

Before the model, is compared with the typical test data, let us first show that for dominant tensile load, the model predicts correct response. For this purpose, the same as for the original Bažant and Prat's microplane model, a single finite element (Fig. 4) is first loaded in tension and subsequently, for different level of constant tensile load, it is loaded by shear. Moreover, it is also checked whether the model for the well

known Willam's test (Willam et al., 1987) yields physically correct results. Finally, it is demonstrated that in the finite element analysis, the model does not cause locking of stresses.

No doubt, it would be more appropriate to test the model on the constitutive level without using finite element. In some cases, finite element could not exactly reproduce the material response. Here we chose the finite element because it is relatively easy to reproduce a complicated stress–strain histories, in which rotating of the principal stress–strain directions takes place during the loading process. If for such a case, the model response is physically correct, what is the main purpose of these tests, it would most probably also be correct on the constitutive level.

4.1.1. Tension and tension-shear test

Fig. 12a shows the calculated stress–strain curves (lateral and axial directions) for uniaxial tensile load. As can be seen, in contrast to the standard kinematic formulation of the model, the new model in lateral direction predicts contraction for the entire load history. This can also be seen from Fig. 12b which shows the ratio between lateral and axial strains (with negative sign) at different load levels. Obviously, by increase of damage in the axial direction the lateral strain decreases asymptotically to zero.

In Fig. 13a, the calculated shear stress–strain curves are plotted for different levels of tensile stresses. As can be seen, in contrast to the original kinematic microplane model (see Fig. 4b), independent of the tensile stress level, the shear stresses are always correctly reduced to zero. The shear strength envelope (yield surface) for different axial tensile stresses, varied in the range of 0 to f_t (uniaxial tensile strength), is plotted in Fig. 13b. As can be seen, it decreases exactly to zero with increase of tensile stresses up to f_t.

4.1.2. Willam's test with rotation of principal directions

To check whether the proposed model predicts consistent solution for tensile dominant load with significant rotations of principal stresses, Willam's test is performed (Willam et al., 1987). In this test, uniaxial tension is applied first in the x direction (plane stress state), reaching the onset of tensile cracking. Subsequently, strain increments are prescribed to all degrees of freedom proportionally to $\Delta\varepsilon = [\Delta\varepsilon_{xx}, \Delta\varepsilon_{yy}, \Delta\gamma_{xy}]^{\mathrm{T}} = [0.50, 0.75, 1.00]^{\mathrm{T}}$. This implies increments of tensile strain for both principal axes, accompanied by a rotation that reaches asymptotically the value of 38°, measured from the x direction. The used material parameters are: $Y = 34\,000$ MPa, $\nu = 0.18$, $f_t = 2.90$ MPa, $f_c = 38.0$ MPa and fracture energy

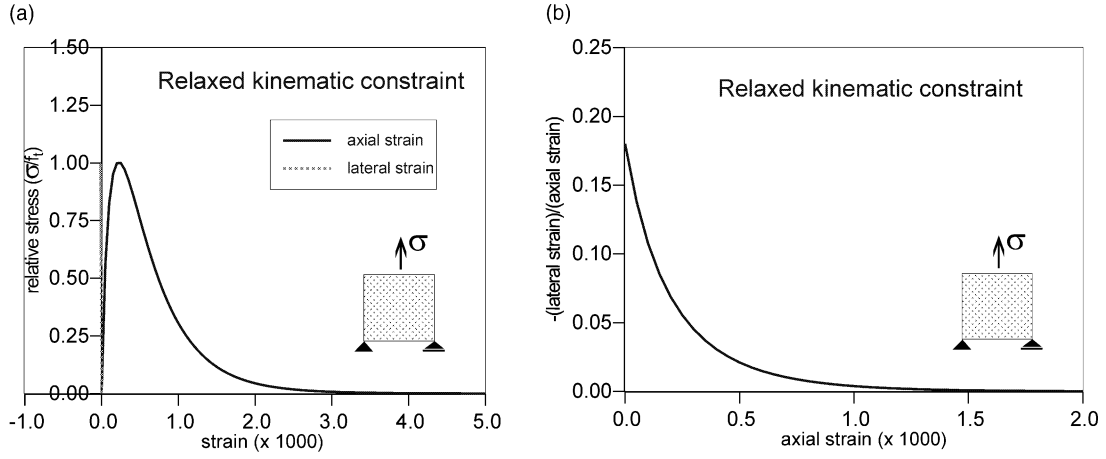

Fig. 12. Uniaxial tension: (a) axial and lateral strains as a function of the relative axial stress and (b) ratio between lateral and axial strain as a function of the axial deformation.

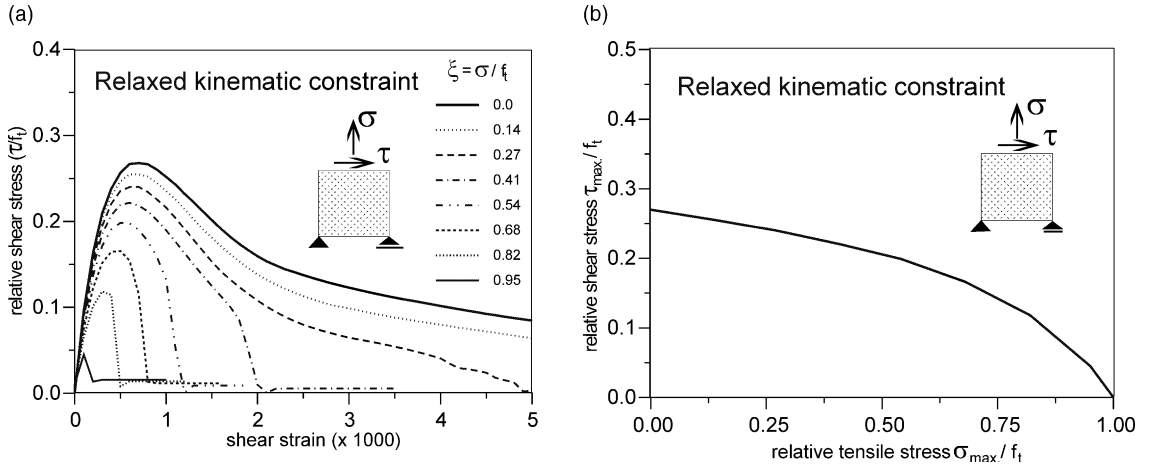

Fig. 13. Tension–shear load combination: (a) shear stress–strain responses for different levels of constant tensile stresses and (b) shear resistance as a function of the tensile stress.

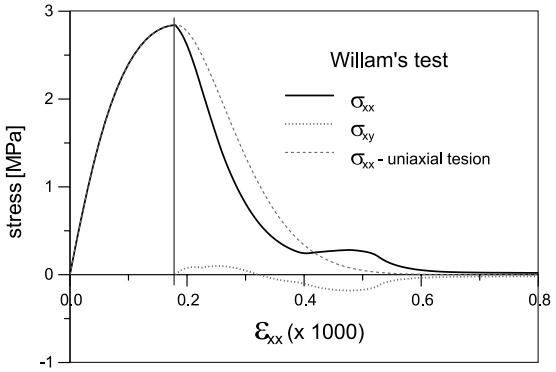

Fig. 14. Willam's test in rotating tension/shear.

$G_F = 0.075$ N mm/mm^2 (assumed crack band = 60 mm). The evolution of σ_{xx} and σ_{xy} is shown in Fig. 14. For comparison, uniaxial stress–strain response is also plotted. As can be seen from Fig. 14, the model prediction is physically correct and qualitatively the same as, for instance, the response obtained by the multicrack model (multisurface elastoplastic formulation; Carol and Bažant, 1995). Compared to the uniaxial tensile response, the multidirectional damage reduces the post-peak capacity in x direction and for large positive strains (tension) all stresses exactly reduce to zero.

4.1.3. Stress-locking test

An important feature of the macroscopic material model for smeared fracture analysis is that the model should not exhibit stress locking. The stress locking may be observed when the finite elements are not parallel with the crack direction. The problem is well known from the finite element fracture analysis when the so called smeared crack models are used (rotated or fixed crack approach, for more details see Jirásek and Zimmerman, 1998). To check if the present model is stress-locking free, a simple three-point bending notched beam is analyzed within the frame work of the crack-band theory (Bažant and Oh, 1983). The

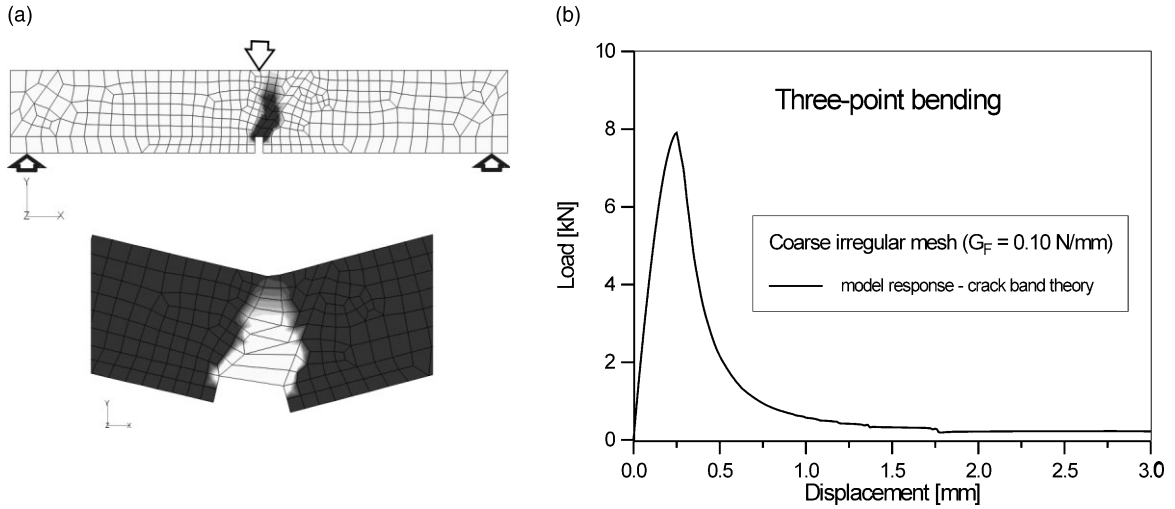

Fig. 15. Three-point bending test: (a) crack pattern (dark zone) in terms of maximum principal strains and (b) mid-span load–displacement curve.

standard fracture properties for normal concrete are adopted. Fig. 15a shows the crack pattern for relatively coarse irregular mesh in terms of the maximum principal strains. The calculated load-midspan displacement is plotted in Fig. 15b. As can be seen, although the mesh is irregular, the load reduces almost exactly to zero i.e. there is no stress locking.

4.2. Comparison with standard test data

The model response for concrete is compared with the typical test data available from the literature. These tests include: (1) uniaxial compression tests of van Mier (1984, 1986), see Fig. 16; (2) uniaxial

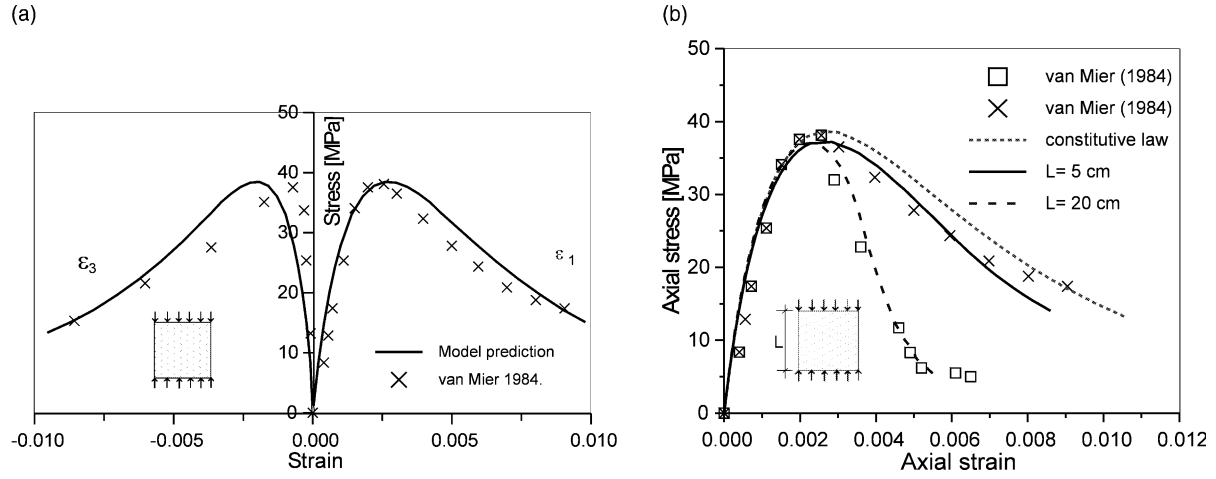

Fig. 16. Uniaxial compression tests of van Mier (1984) and model prediction: (a) material model level (point property) and (b) modeling of the test specimen using three-dimensional finite elements in the framework of the crack band theory.

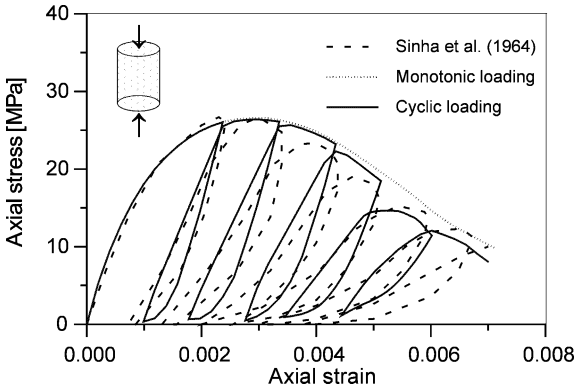

Fig. 17. Uniaxial compression monotonic and cyclic test of Sinha et al. (1964) and the model prediction – three-dimensional finite element simulation.

compression tests for monotonic and cyclic loading of Sinha et al. (1964), see Fig. 17; (3) uniaxial tensile tests for monotonic and cyclic loading of Reinhardt and Cornelissen (1984), see Fig. 18; (4) biaxial tension-compression tests of Kupfer et al. (1969), see Fig. 19 and shear-compression failure envelope measured by Bresler and Pister, (1958), see Fig. 20 and Goode and Helmy (1967), see Fig. 20; (5) cyclic shear test of Eligehausen et al. (1983), see Fig. 21 and (6) monotonic and cyclic triaxial compression test data of US Army Engineers Waterways Experiment Station (USAE-WES, 1994, Figs. 22 and 23; taken from Bažant et al., 1996a,b).

Generally, the microplane parameters were calibrated such that e_1 and m were obtained from the fit of the uniaxial tensile test, e_2, e_3, n and k are obtained from the uniaxial compressive test data with the assumption that e_1 and m are independent of the parameters e_2, e_3, n, k. The ratio between the initial deviatoric and volumetric moduli is assumed to be $\eta = 0.8$–1.0. The parameter e_4, which controls the normal-shear interaction on microplanes, is taken as constant and $e_4 = 4$. The volumetric compression is controlled by parameters a, b, p, q. They are assumed to be constant and are obtained by the fit of the volumetric compression test data.

Fig. 16 shows the results of the uniaxial compression tests of van Mier (1984, 1986). The results are compared with the model prediction. The plotted stresses and strains are average values over the specimen height. Three different heights (h) of the test specimen were considered ($h = 50$, 100 and 200 mm). The material model is calibrated based on the test data of the smallest specimen ($h = 50$ mm). The basic material properties were approximately the same as in the experiment: $Y = 45\,000$ MPa, $\nu = 0.18$, uniaxial tensile strength $f_t = 3.8$ MPa, uniaxial compressive strength $f_c = 32$ MPa. The corresponding model parameters are: $e_1 = 0.00010$, $e_2 = 0.0010$, $e_3 = 0.0012$, $m = 1.0$, $n = 0.9$, $k = 0.9$, $\eta = 0.8$. Fig. 16a shows the model prediction and the corresponding experimental results for the specimen height $h = 50$ mm.

The structural effect which was observed in the experiment is also studied. In the three-dimensional numerical simulation two different specimen sizes were considered ($h = 50$ and 200 mm). The size of the finite elements was chosen such that the concrete fracture energy $G_F = A_f c_b$ with A_f, area under the uniaxial tensile stress–strain relationship and c_b, crack band width (approximately the average size of the adopted finite element). To assure the objectivity of the analysis with respect to the element size, the size of the elements was the same in both examples. Plane stress finite element analysis is carried out assuming a few weak elements in the mid of the specimen (tensile strength is reduced for about 10%) in order to initiate the localization of damage and account for the nonuniformity of the stress field as a consequence of concrete heterogeneity. Fig. 16b shows the comparison between the experimental results and the model prediction. Similar to the tests, the analysis shows no significant structural effect in the pre-peak regime and strong

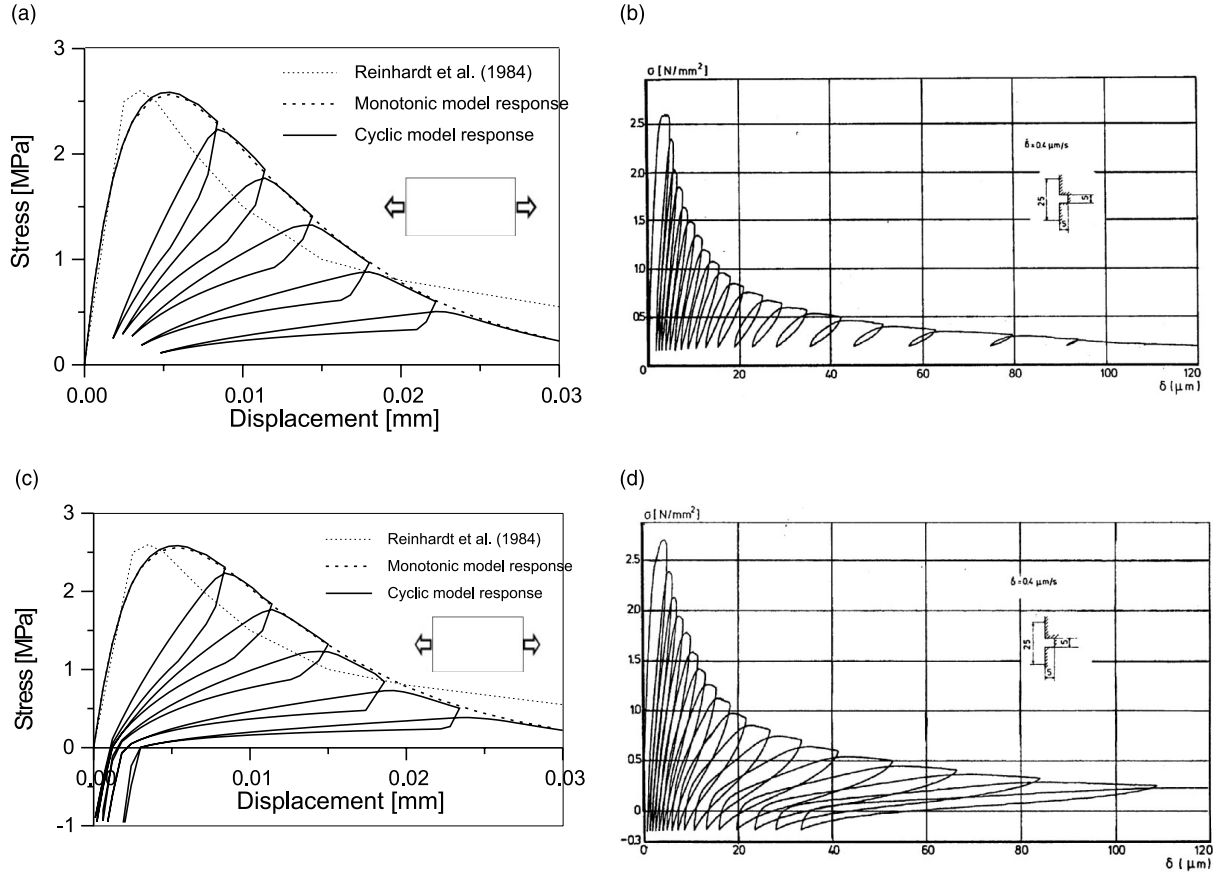

Fig. 18. Uniaxial tensile monotonic and cyclic tests of Reinhardt and Cornelissen (1984) – model prediction and test results for: (a,b) loading, unloading close to zero and reloading, (c,d) loading, unloading in compression (5% of uniaxial compressive strength f_c) and again reloading, (e,f) loading, unloading in compression (25% of f_c) and again reloading.

structural effect on the post peak response. For comparison, the response with no structural effect (constitutive law) is also plotted. As can be seen, the pre-peak response is nearly the same as in the FE analysis, which means no structural effect is present, however, the post-peak response is size dependent. Fig. 16b indicates a good agreement between the test and analysis.

In Fig. 17, the test data (Sinha et al., 1964) and calculated curves for uniaxial cyclic compression are shown and compared. Since the post-peak response is not material but structural property, three-dimensional finite element analysis (1/4 of the cylinder test specimen was modeled) is carried out. The model parameters were calibrated by fitting the results of monotonic load by the three-dimensional FE simulation. They were set as $Y = 27\,500$ MPa, $v = 0.18$, $f_t = 2.35$ MPa, $f_c = 24.5$ MPa. The corresponding model parameters are: $e_1 = 0.00007$, $e_2 = 0.0013$, $e_3 = 0.0015$, $m = 1.0$, $n = 0.82$, $k = 0.82$, $\eta = 0.8$. Fig. 17 shows a good agreement between the test and calculated data. For instance, the calculated cyclic response (envelope) approximately follows the monotonic response, same as that observed in the test. Furthermore, as in the experiment, by unloading and repeated reloading, the drop of the peak stresses was observed.

The test results of Reinhardt and Cornelissen (1984) for uniaxial tensile monotonic and cyclic loading are compared with the model prediction. Three different loading–unloading regimes were employed:

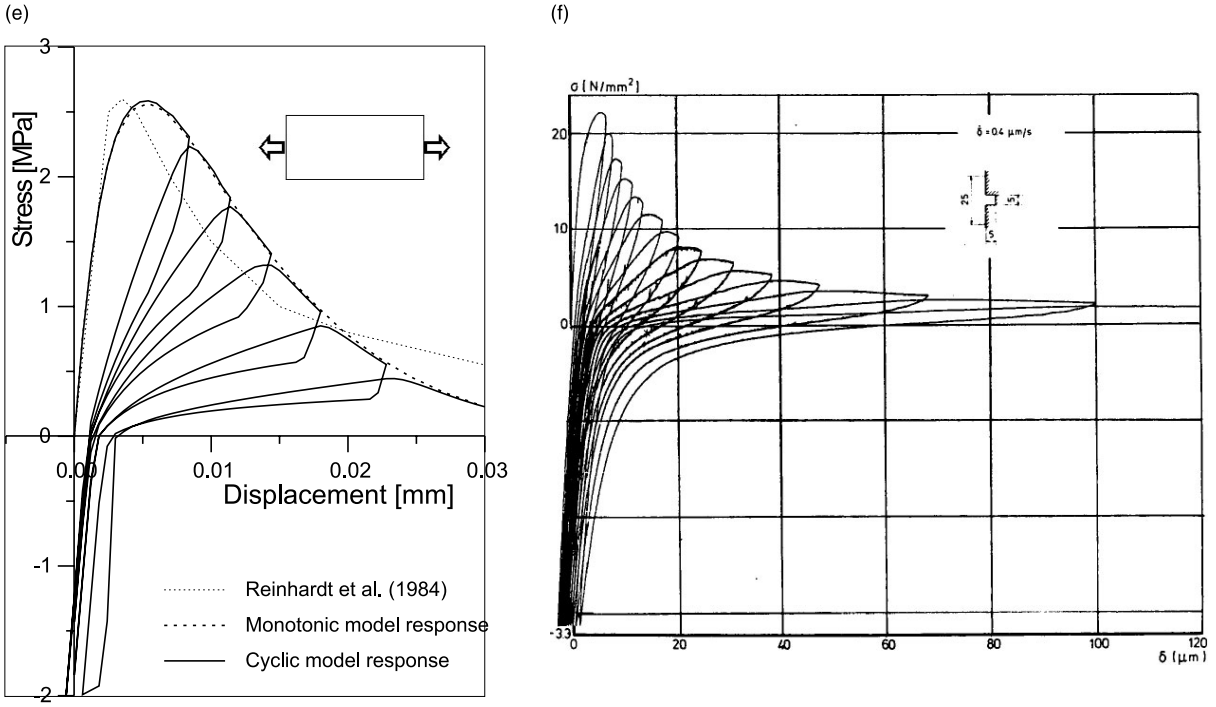

Fig. 18. *(continued)*

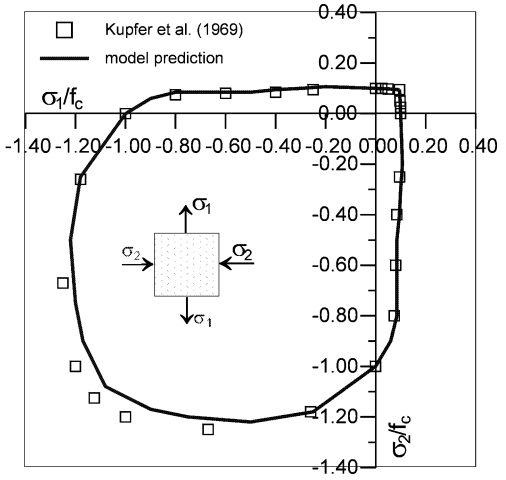

Fig. 19. Biaxial principal stress failure envelope, test data of Kupfer et al. (1969) and the model prediction.

(a) Loading in tension, unloading close to zero stress and reloading in tension; (b) loading in tension, unloading into compression up to approximately 5% of the uniaxial compressive strength and reloading in tension and (c) loading in tension, unloading in compression up to approx. 25% of the uniaxial compressive strength and reloading in tension. For simplicity reasons, the analysis was carried out on a unit three-dimensional finite element. In the experiments, the strains were measured over the specimen length of

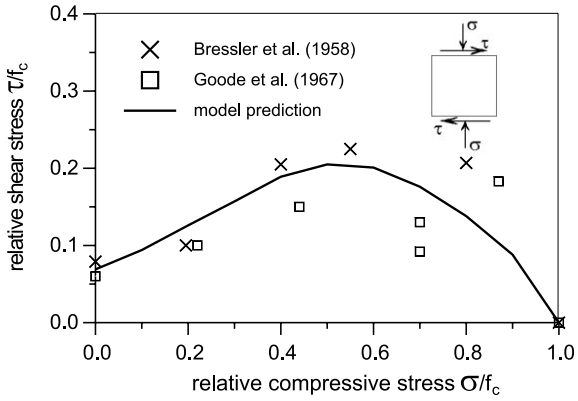

Fig. 20. Compression–Shear failure envelope, test data of Bresler et al. (1958) and Goode et al. (1967) vs. model prediction.

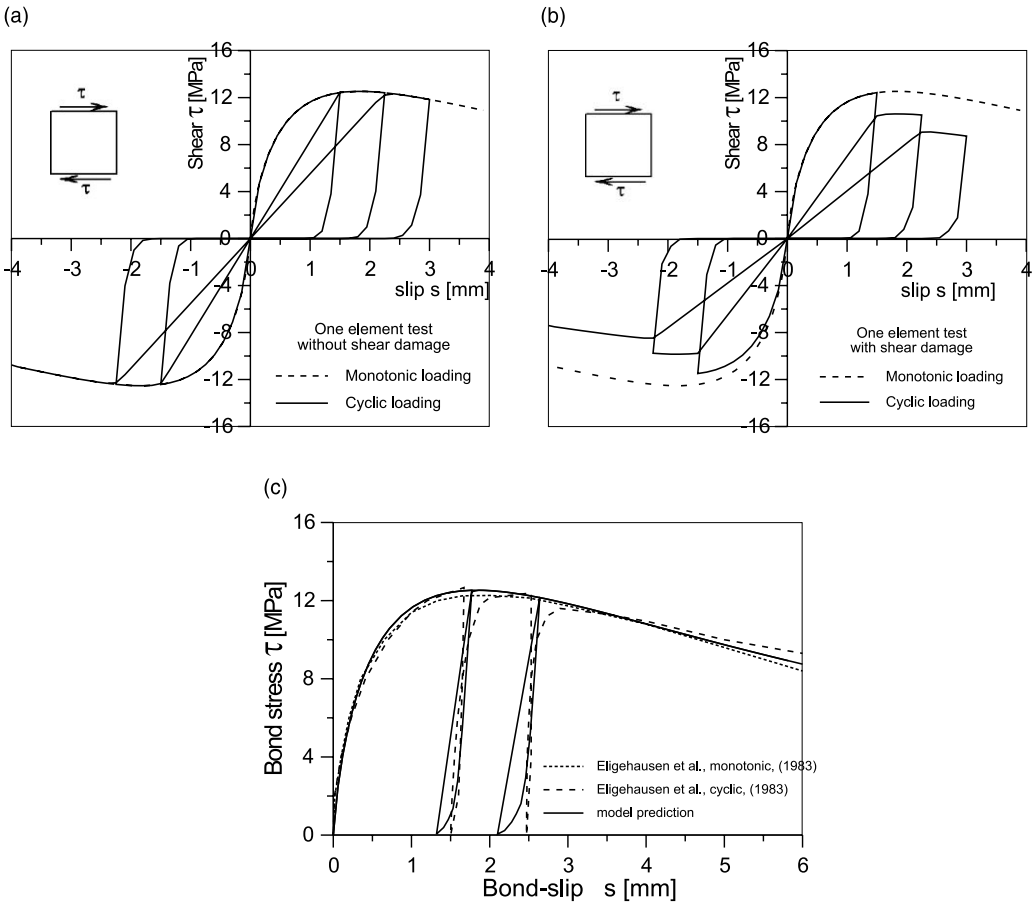

Fig. 21. Shear response: (a) material model level without cyclic shear damage, (b) with cyclic shear damage, (c) model response compared with test data of Eligehausen et al. (1983).

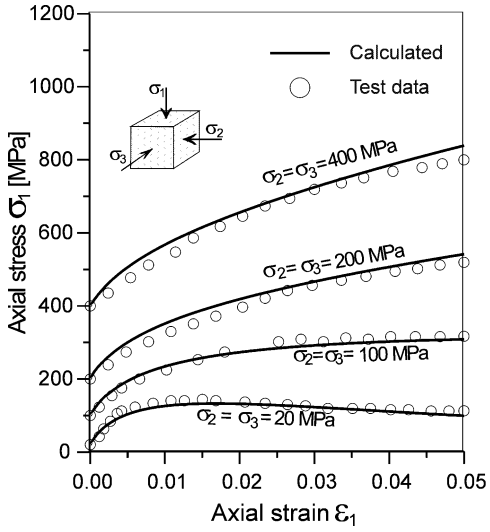

Fig. 22. Triaxial compression test data (USAE-WES 1994; taken from Bažant et al. (1996)) and the model prediction.

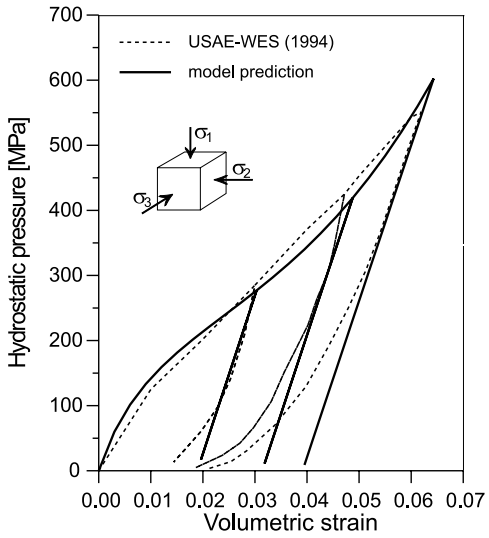

Fig. 23. Hydrostatic cyclic loading conditions – test data (USAE-WES, taken from Bažant et al. (1996)) and the model response.

25 mm. Based on the test report, the material model parameters were set as: $Y = 34\,700$ MPa, $\nu = 0.18$, $f_t = 2.6$ MPa, $f_c = 44.5$ MPa. The corresponding model parameters are: $e_1 = 0.000072$, $e_2 = 0.0022$, $e_3 = 0.0025$, $m = 1.0$, $n = 1.0$, $k = 1.0$, $\eta = 1$. Fig. 18 shows the measured and calculated stress–strain curves. As can be seen, for all load combinations, the model predicts similar response as observed in the experiments.

Two dimensional test failure data (tension–tension, tension–compression and compression–compression, see Kupfer et al. (1969)) and compression–shear failure envelope (Bresler et al., 1958 and Goode and

Helmy, 1967) are shown in Figs. 19 and 20. The material model parameters were approximately the same as in the experiments: (a) tests of Kupfer et al.: $Y = 30\,000$ MPa, $v = 0.18$, $f_t = 2.9$ MPa, $f_c = 32.4$ MPa; the corresponding model parameters are: $e_1 = 0.00008$, $e_2 = 0.0012$, $e_3 = 0.0015$, $m = 1.5$, $n = 1.0$, $k = 1.0$, $\eta = 1.0$; and (b) compression–shear test: $Y = 30\,000$ MPa, $v = 0.18$, $f_t = 1.8$ MPa, $f_c = 31.8$ MPa; the corresponding model parameters are: $e_1 = 0.00005$, $e_2 = 0.0018$, $e_3 = 0.0020$, $m = 1.5$, $n = 1.5$, $k = 1.5$, $\eta = 0.95$. As can be seen from Figs. 19 and 20, the agreement between the model prediction and the test data is good.

Furthermore, the model response for monotonic and cyclic shear load with prevented dilatancy (simple shear) was checked. Such a load combination approximately corresponds to the pull-out of a ribbed steel bar from a concrete block. Therefore, the model prediction is compared with the experimental results of Eligehausen et al. (1983). The material properties were set as follows: $Y = 25\,000$ MPa, $v = 0.18$, $f_t = 2.75$ MPa, $f_c = 28.0$ MPa. The corresponding model parameters are: $e_1 = 0.00006$, $e_2 = 0.0008$, $e_3 = 0.0010$, $m = 0.50$, $n = 0.50$, $k = 0.50$, $\eta = 0.8$. The constitutive law for cyclic shear response, once with and once without accumulated cyclic damage with the use of Eq. (22), are shown in Figs. 21a and, b. In Fig. 21c, the model response is compared with the test data. As can be seen, the prediction agrees well with the experimental results.

Finally, the model was calibrated and checked for triaxial compression load using the test data obtained at USAE-WES (1994) (taken from Bažant et al. (1996)). The concrete properties were: $Y = 35\,000$ MPa, $v = 0.18$, $f_c = 45.5$ MPa and the corresponding model parameters are: $e_1 = 0.0001$, $e_2 = 0.002$, $e_3 = 0.0022$, $e_4 = 4.0$, $m = 1.0$, $n = 0.65$, $k = 0.65$ and $\eta = 0.8$. Fig. 22 shows a good agreement between the experimental results and the model predictions. In addition, Fig. 23 shows the comparison between the model response for hydrostatic loading–unloading case and the corresponding test results. As may be seen the agreement is again good.

For practical applications, Young's modulus and Poisson's ratio are assumed to be concrete macroscopic properties and the model parameters are adopted as follows. From volumetric compression test a set of parameters is obtained: $a = 0.005$, $b = 0.043$, $p = 0.75$, $q = 2.00$ and $e_4 = 4.0$. These parameters are taken as constant and independent of the concrete type. Parameters e_1 and m are obtained by fitting into the uniaxial tensile stress–strain relationship, both control tensile strength and the area under the uniaxial tensile stress–strain curve. The parameters e_2, e_3, n and k control the uniaxial compressive strength as well as the area under the uniaxial compressive constitutive law. Based on the fit of a number of test data the following is adopted: $e_2 = e_3$ and $k = 0.85n$. The optimal value for the ratio between the initial deviatoric and volumetric modulus is found to be $\eta = 0.8$. In total, besides Young's modulus and Poisson's ratio, there is only four independent model parameters. The parameters which control the cyclic response of the model Eq. (21) are constant, independent of the concrete properties and the same for each microplane strain component (Table 1). All model parameters can physically be interpreted, however, there is no explicit relation with concrete macroscopic properties and therefore they have to be obtain by fitting of the test data.

Table 1
Model parameters for cyclic load control

Strain component		$\alpha, \varepsilon \leqslant \varepsilon_p$	$\alpha, \varepsilon > \varepsilon_p$	β
Volumetric	Positive	1.0	0.1	0.2
	Negative	1.0	–	–
Deviatoric	Positive	1.0	1.0	0.2
	Negative	1.0	1.0	0.5
Shear	Positive	1.0	1.0	0.5
	Negative	1.0	1.0	0.5

5. Conclusions

The present microplane model is the macroscopic three-dimensional material model for concrete. The model is aimed to be used for modeling of damage and fracture phenomena in concrete and reinforced concrete structures loaded under general three-dimensional state of stresses and strains.

The simplest and computationally most efficient form of the model formulation is based on the kinematic constraint approach which, however, in combination with realistic stress–strain relationships for concrete leads to pathological model response for dominant tensile load. It is demonstrated that the main reason for pathological behavior of kinematic constrained microplane (Bažant and Prat, 1988) subjected to tension is related to the split of the normal microplane component into volumetric and deviatoric part and not to the kinematic constraint itself. Consequently, the improved model can also be based on the kinematic constraint approach.

The improvement of the model is accomplished by the relaxation of the kinematic constraint for dominant tensile load, i.e. on the microplane level, the kinematic constraint is relaxed by splitting of the microplane strain component into the effective and relaxed part. The split is controlled by the discontinuity function which depends on the total volumetric strain and maximal principal stress. The physical background of the concept is based on the fact that for the localization of tensile damage, the stresses and strains on the microplanes which are perpendicular to the damage (crack) direction approximately relaxed to zero. It is demonstrated that the new model predicts physically correct results.

The conceptual simplicity of the new model is preserved, i.e. for the fixed set of microplanes and for the already defined uniaxial microplane stress–strain relationships, the microplane stresses are calculated directly from effective microplane strains. Using relatively simple cyclic rules on the microplane level, the macroscopic cyclic response for any three-dimensional stress–strain state is automatically brought out. Moreover, it is shown that the model can relatively easy account for the initial anisotropy.

Comparison with the test data shows that the model is able to realistically predict concrete response for different stress–strain combinations (tension, compression and shear) as well as for cyclic load histories. In the finite element implementation, the model does not exhibit stress locking. Same as that for any macroscopic model for quasi-brittle materials, to prevent localization of damage into a zero volume and to assure mesh objective results of the smeared fracture finite element analysis, the model has to be coupled with the so-called localization limiter (crack band approach or higher order methods).

In general, the model has 15 parameters. Although these parameters have physical interpretation, none of them is explicitly related to the macroscopic material properties of concrete. Consequently, the calibration is empirical and based on the available experimental data. For normal concrete, most of the parameters can be taken constant i.e. besides basic macroscopic concrete properties (Young's modulus and Poisson's ratio) only four additional parameters need to be set by fitting into test data. For practical applications, the computer code has been written which for given macroscopic concrete properties automatically generates the microplane model parameters.

References

Batdorf, S.B., Budianski, B., 1949. A mathematical theory of plasticity based on the concept of slip. Technical Note No. 1871, National Advisory Committee for Aeronautics, Washington, DC.

Balazs, G.L., 1991. Fatigue of bond. ACI Materials Journal 88 (6), 620–629.

Bažant, Z.P., Oh, B.-H., 1983. Crack band theory for fracture of concrete. Materials and Structures, RILEM 93 (16), 155–177.

Bažant, Z.P., 1984. Size effect in blunt fracture: Concrete, rock, metal. Journal of Engineering Mechanics, ASCE 110 (4), 518–535.

Bažant, Z.P., Gambarova, P., 1984. Crack shear in concrete: Crack band microplane model. Journal of Engineering Mechanics, ASCE 110, 2015–2035.

Bažant, Z.P., Oh, B.-H., 1986. Efficient numerical integration on the surface of a sphere. Zeitschrift für angewandte Mathematik und Mechanik, ZAMM 66 (1), 37–49.

Bažant, Z.P., Prat, P., 1987. Creep of anisotropic clay: new microplane model. Journal of Engineering Mechanics, ASCE 103 (7), 1050–1064.

Bažant, Z.P., Prat, P.C., 1988. Microplane model for brittle-plastic material, -parts I and II. Journal of Engineering Mechanics, ASCE 114, 1672–1702.

Bažant, Z.P., Ožbolt, J., 1990. Nonlocal microplane model for fracture, damage and size effect in structures. Journal of Engineering Mechanics, ASCE 116 (11), 2485–2504.

Bažant, Z.P., 1991. Why continuum damage is nonlocal: micromechanics arguments. Journal of Engineering Mechanics, ASCE 117 (5), 1070–1087.

Bažant, Z.P., Xiang, Y., Prat, P.C., 1996a. Microplane model for concrete I. Stress–strain boundaries and finite strain. Journal of Engineering Mechanics, ASCE 122 (3), 245–262.

Bažant, Z.P., Xiang, Y., Adley, M., Prat, P.C., Akers, S., 1996b. Microplane model for concrete- II. Data delocalization and verification. Journal of Engineering Mechanics, ASCE 122 (3), 263–268.

Bažant, Z.P., Caner, F.C., Carol, I., Adley, M.D., Akers, S.A., 1998. Microplane model M4 for concrete. Internal Report 98-12/407m (Part I), Department of Civil Engineering, Northwestern University. Journal of Engineering Mechanics, ASCE, submitted for publication.

de Borst, R., 1991. Continuum models for discontinuous media. Proceedings of the International RILEM/ESIS Conference on Fracture processes in concrete, rock and ceramics, Noordwijk, The Netherlands, pp. 601–618.

Bresler, B., Pister, K.S., 1958. Strength of concrete under combined stresses. Journal of ACI 551 (9), 321–345.

Carol, I., Bažant, Z.P., Prat, P., 1991. Geometric damage tensor based on the microplane model. Journal of Engineering Mechanics, ASCE 117 (10), 2429–2448.

Carol, I., Prat, P., Bažant, Z.P., 1992. New explicit microplane model for concrete: theoretical aspects and numerical implementation. International Journal of Solids and Structures 29 (9), 1173–1191.

Carol, I., Bažant, Z.P., 1995. New developments in microplane and multicrack models for concrete. Fracture Mechanics of Concrete Structures. In: Wittmann, F.H. (Ed.), vol. 2. AEDIFICATIO Publishers, Fréiburg, Germany, pp. 841–855.

Carol, I., Bažant, Z.P., 1997. Damage and plasticity in microplane theory. International Journal of Solids and Structures 34 (29), 3807–3835.

Chen, A.C.T., Chen, W.F., 1975. Constitutive relations for concrete. Journal of Engineering Mechanics, ASCE 101 (4), 465–481.

Eligehausen, R., Popov, E.P., Bertero, V.V., 1983. Local bond stress-slip relationships of deformed bars under generalized excitations. Report No. UCB/EERC-83/23. Earthquake Engineering Research Center, College of Engineering, University of California, Berkeley, CA.

Eligehausen, R., Ožbolt, J., 1998. Size Effect in Design of Fastenings. In: Pijaudier-Cabot, G., Bittnar, Z., Gérard, B. (Eds.), Mechanics of Quasi-Brittle Materials and Structures, HERMES, pp. 95–118.

Gerstle, K.H., Aschl, H., Bellotti, R., Bertacchi, P., Kotsovos, M.D., Ko, H.Y., Linse, D., Newman, J.B., Rossi, P., Schickert, G., Taylor, M.A., Traina, L.A., Wrinkler, H., Zimmerman, R.M., 1980. Behavior of concrete under multiaxial stresses. Journal of Engineering. Mechanics, ASCE 106 (6), 1383–1403.

Gerstle, K.H., 1981. Simple formulation of biaxial concrete behaviour. Journal of ACI 78 (1), 62–68.

Goode, C.D., Helmy, M.A., 1967. The strength of concrete under combined shear and direct stress. Magazine of Concrete Research 19 (59), 105–112.

Jirásek, M., 1993. Modeling of Fracture and Damage in Quasibrittle Materials. Doctoral Dissertation, Northwestern University.

Jirásek, M., Zimmerman, T., 1998. Rotating crack model with transition to scalar damage. Journal of Engineering Mechanics, ASCE 124 (3), 277–284.

Jirásek, M., 1998. Embedded crack models for concrete. Workshop on Modeling of Plain and Reinforced Concrete. University of Stuttgart, Germany.

Kupfer, H., Hilsdorf, H.K., Rsch, H., 1969. Behavior of concrete under biaxial stresses. Journal of ACI 66, 656–666.

Li, Y.-J., Ožbolt, J., Eligehausen, R., 1998. Size Effect on the Concrete Compression Failure Load. In: Mihashi, H., Rokugo, K. (Eds.), Fracture Mechanics of Concrete Structures, vol. 3, 1983–1992.

van Mier, J.G.M., 1984. Strain-softening of concrete under multiaxial loading conditions. Dissertation, Eindhoven University of Technology.

van Mier, J.G.M., 1986. Multiaxial strain-softening of concrete. Part I: fracture. Part II: load histories. Materials and Structures, RILEM 111 (19), 179–200.

Ortiz, M.A., 1985. A constitutive theory for the inelastic behavior of concrete. Mechanics of Materials 4, 67–93.

Ožbolt, J., Bažant, Z.P., 1992. Microplane model for cyclic triaxial behavior of concrete. Journal of Engineering Mechanics, ASCE 118 (7), 1365–1386.

Ožbolt, J. 1995., Maßstabseffekt und Duktilität von Beton-und Stahlbeton Konstruktionen. Postdoctoral Thesis, Stuttgart University.

Ožbolt, J., Bažant, Z.P., 1996. Numerical smeared fracture analysis: Nonlocal microcrack interaction approach. International Journal of Solids and Structures 39 (4), 635–661.

Ožbolt, J., Li, Y.-J., Eligehausen, R., 1997. 3D-Analyse von Balken-Stützen Verbindungen aus Normal-und Hochfestem Beton unter Zyklischer Beanspruchung. Beton-und Stahlbetonbau, vol. 93, Heft 4.

Ožbolt, J., Li, Y.-J., Eligehausen, R., 1998. 3D cyclic finite element analysis of beam-column connections. In: Mihashi, H., Rokugo, K. (Eds.), Fracture Mechanics of Concrete Structures, vol. 3, pp. 1523–1536.

Ožbolt, J., Asmus, J., Jebara, K., 1999a. Splitting of concrete block caused by inside pressure-failure mechanism and size effect. In: Pijaudier-Cabot, G., Bittnar, Z., Gérard, B. (Eds.) Mechanics of Quasi-Brittle Materials and Structures. HERMES, pp. 272–288.

Ožbolt, J., Mayer, U., Vocke, H., Eligehausen, R., 1999b. Verschmierete Rismethode. Beton-und Stahlbetonbau, vol. 94, Heft 10.

Ožbolt, J., Meštrović, D., Li, Y.-J., Eligehausen, R., 2000. Compression failure – beams made of different concrete types and sizes. Journal of Structural Engineering, ASCE 126 (3), 200–209.

Pijaudier-Cabot, G., Bažant, Z. P., 1987. Nonlocal damage theory. Journal of Engineering Mechanics, ASCE 113 (10), 1512–1533.

Prat, P.C., Gens, A., 1994. Microplane formulation for quasibrittle materials with anisotropy and damage. In: Bažant, Z., Bittnar, Z., Jirásek, M., Mazars, J. (Eds.) Fracture and damage in quasibrittle structures. E & Spon, pp. 67–74.

Reinhardt, H.W., Cornelissen, H.A.W., 1984. Post-peak cyclic behaviour of concrete in uniaxial tensile and alternating tensile and compressive loading. Cement and Concrete Research 14, 263–270.

Sinha, B.P., Gerstle, K.H., Tulin, L.G., 1964. Stress–strain relations for concrete under cyclic loading. Journal of ACI 62 (2), 195–210.

Taylor, G.I., 1938. Plastic strain in metals. Journal of the Institute of Metals 62, 307–324.

Willam, K.J., Warnke, E.P., 1974. Constitutive model for triaxial behavior of concrete. Seminar on Concrete Structures Subjected to Triaxial Stresses. Int. Assoc. of Bridge and Struct. Engng. Conf., Bergamo, Italy.

Willam, K.J., Pramono, E., Sture, S., 1987. Fundamental issues of smeared crack models. In: Shah, S., Swartz, S. (Eds.), SEM-RILEM Int. Conf. on Fracture of Concrete and Rock, pp. 192–207.

Willam, K.J., Hansen, E., Kang, H.D., 1999. Performance evaluation of damage and plasticity formulations for concrete. Seminar on Post-Peak Behavior of RC Structures Subjected to Seismic Loads – Recent Advances and Challenges on Analysis and Design. Japan Concrete Institute, Tokyo, Japan, pp. 23–41.